cord and nerve roots, sometimes causing severe myeloradiculopathy. The cause of this disease is not known, but recent reports indicate the possibility of an association between the onset of the condition and the genetic background [39]. Previous immunohistochemical studies showed the local expression of BMP and its receptors in surgical specimens of ossification of the ligamentum flavum (OLF) [40] and ossification of the posterior longitudinal ligament [41], and suggest the possible involvement of BMP in the pathogenesis of this ossification.

Many patients with ossification of the spinal ligament have subclinical conditions [42]; symptomatology depends on the degree of the narrowing of the canal caused by the increased ossified mass [43]. Therefore, identifying local candidate factors involved in the progression of the condition is important. We studied the involvement of CDMP-1 in OLF tissues, by immunohistochemistry and in situ hybridization [44]. CDMP-1 was synthesized by fibroblasts and chondrocytes in the ossified regions, whereas it was not detected in nonossifying regions (Fig. 10). CDMP-1 has been reported as factor promoting chondrogenesis [11]; the findings suggest that CDMP-1 may be involved in the progression of ossification. CDMP-1 may become a therapeutic target for the progression of ossification of the spinal ligament.

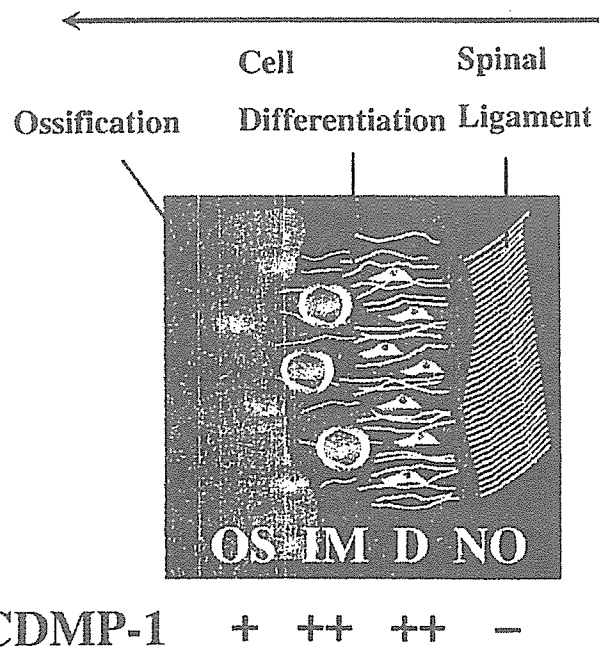

Fig. 10. Proposed model of the localization of CDMP-1 mRNA and protein in the cellular mechanisms of progression of ossification of the ligamentum flavum (OLF). CDMP-1 mRNA and protein are not localized in cells in the nonossifying regions (*NO*), whereas CDMP-1 is localized in fibroblastic cells in the zone initiating ossification distant from the ossification front (*D*), in chondrocytes in the intermediate zone (*IM*), and in cells in the ossification front (*OS*)

Benign tumorous conditions: osteochondroma and osteoid osteoma

Osteochondroma, also known as an exostosis, is one of the common benign tumorous conditions in skeletal disorders. The condition is characterized by the formation of new osteochondrogenic tissue, called a "cartilage cap" [45] (Fig. 11). The outer growth of a cartilage cap sometimes leads to orthopedic problems such as pain, limitation of range of motion, and compression of neurovascular structures. Our previous studies [46,47] showed that BMP-2 and BMP-4 proteins and mRNAs were identified within mesenchymal cells positive for type III collagen in the outer layer of the cartilage cap, and within chondrogenic cells positive for type II collagen in the inner layer BMPR IB mRNA, a receptor for BMP-2 and -4, has been identified in the chondrocytes in the inner layer (Fig. 12). These findings suggest the possible action of BMP-2/4-BMPR IB pathways in the pathogenesis underlying the growth of osteochondromas, and BMP-2 and -4 could become target molecules for the treatment of osteochondromas.

In addition, the involvement of BMP-2 and -4 in another benign bone tumor has been reported [47,48]. Osteoblastoma is one of the benign tumorous conditions characterized by an osteoid nidus. The nidus is located within the center of the tumor, surrounded by sclerotic bone formed due to an osteoblastic response within the nidus. BMP-2 and -4 have been immunohistochemically identified in cells in the nidus, suggesting the possible involvement of BMP-2 and -4 in the osteoblastic reaction.

Osteoarthritis (OA)

Osteoarthritis (OA) is a common orthopedic disease based on the age-related regeneration of joint cartilage; regenerative changes in the articular cartilage, as well as osteophyte formation, are the essential characteristics of the condition (Fig. 13).

The localization and expression of BMP-2 and -4 have been extensively studied by in situ hybridization and immunohistochemistry [49]. BMP-2 and BMP-4 mRNA and protein were scarcely detected in normal adult articular

Fig. 11A,B. Radiographic findings showing osteochondroma. **A** X-ray showing osteochondroma expanding on the cortical bone (*arrow*). **B** Magnetic resonance imaging (MRI) showing cartilage cap (*arrow*)

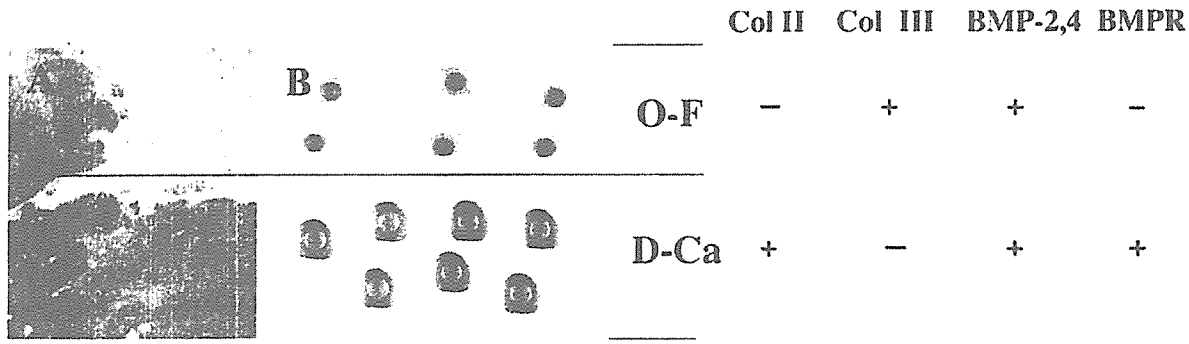

Fig. 12. **A** Histology and **B** illustrations, showing the localization of BMP-2 and -4 in the cartilage cap of osteochondroma. The cartilage cap consists of an outer fibrous (*O-F*) layer and a deep cartilage (D-Ca) layer. The OF layer is composed of fibroblastic cells positive for type III collagen mRNA (*Col III*), and the D-Ca layer is composed of chondrocytes positive for type II collagen mRNA (*Coll II*). BMP-2 and -4 mRNAs and protein are localized in cells in the O-F and D-Ca layers, whereas BMPR (*BMP receptor type IB*) mRNA is localized in cells in the D-Ca layer, but not in the O-F layer. **A** Safranin-O and fast green staining, ×40; *dark area* indicates cartilaginous matrix

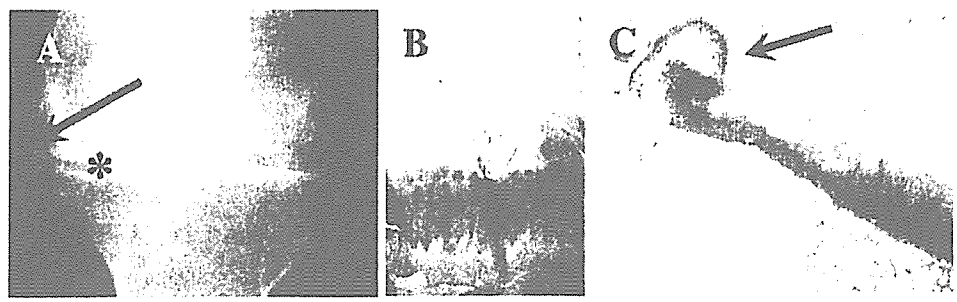

Fig. 13. **A** Radiograph and **B** and **C** histologic characteristics of osteoarthritis (OA). **A** X-ray showing osteophyte formation (*arrow*), as well as narrowing of the width of the articular cartilage *asterisk*. **B** and **C** Histology, showing degenerative changes of OA cartilage (**B**) and newly formed osteo- and chondrogenic tissue, called osteophyte formation (*arrow* in C). **B** and **C** Safranin-O and fast green staining (B: ×40, C: macroscopic magnification)

Table 1. Expression and localization of bone morphogenetic protein (BMP)-2 mRNA in osteoarthritis (OA) cartilage cells

Grade of OA cartilage	Zones		
	Upper	Middle	Deep
Moderately damaged	++ to +++	++ to +++	− to +
Severely damaged	No upper zone	++ to +++	++ to +++

cartilage. However, BMP-2 and BMP-4 mRNA and protein were localized in chondrocytes in damaged OA cartilage (Table 1). In moderately damaged OA cartilage, BMP-2 and -4 were localized in OA cells in the upper and middle zones. However, in severely damaged OA cartilage, they were detected in OA cells even in the deep zone. These findings suggest that the zone-specific distribution of BMP-2 and -4 may be dependent on the degree of OA damage, and that BMP-2 and -4 may be induced in response to the damage to articular cartilage (Fig. 14) [49]. Current findings indicate the induction of the *BMP* gene in cells in damaged OA cartilage. Our unpublished observations, by RT-PCR and western blotting using specific probes, have confirmed the expression and the presence of BMP-2 in OA cartilage.

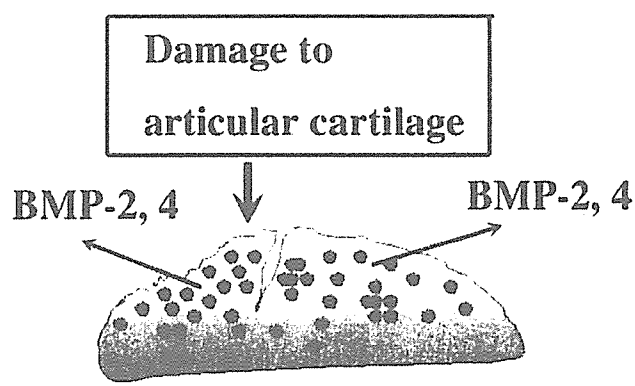

Fig. 14. Proposed mechanisms of BMP induction in damaged OA cartilage. BMP-2 and -4 are induced in OA cells in response to the damage to OA cartilage

Such induction of the *BMP* gene in response to stimuli to cartilage is similar to that observed in fracture healing. Unlike the case in bone repair, spontaneous repair of damaged articular cartilage is rarely observed. The activation of BMP in damaged OA cells does not lead to cartilage repair, despite BMP's chondrogenic activity. Further investigations may aid in our understanding of the downstream mechanisms involved in BMP signaling.

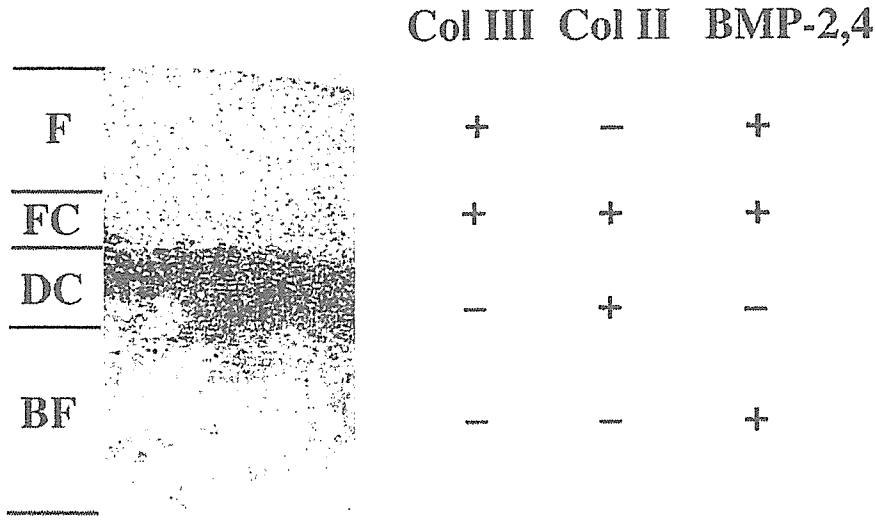

Fig. 15. Localization of BMP-2 and -4 in osteophyte cells. The osteophyte is composed of four distinct layers, i.e., the fibrous (*F*) layer, fibrocartilage (*FC*) layer, deep cartilage (*DC*) layer, and the bone-forming (*BF*) layer. The F layer is composed of fibroblastic cells positive for type III collagen (*Col III*), the FC layer is composed of fibrochondrocytes positive for type II (*Col II*) and type III collagen (*Col III*), the DC layer is composed of chondrocytes positive for type II collagen (*Col II*), and the BF layer is composed of osteoblasts. BMP-2 and -4 are localized in cells in the F, FC, and BF layers, but not in cells in the DC layer

Histologically, findings in the osteophyte are characterized by new bone/cartilage formation resembling endochondral ossification. BMP-2 and -4 mRNAs and proteins are detected in fibroblastic cells, fibrochondrocytes, immature chondrocytes and osteoblasts within the osteophyte tissue in human specimens. BMP-2 and -4 were not detected in mature chondrocytes [49]. In osteophytes, the fibroblasts and fibrochondrocytes were positive for collagen III mRNA; the fibrochondrocytes were also positive for collagen II mRNA, as were immature chondrocytes (Fig. 15). These findings suggest possible roles of BMP-2 and -4 in the early chondrogenic reactions of osteophyte formation.

Conclusion

Several members of the BMP family, such as BMP-2, -4, -7 (OP-1), and GDF-5 (CDMP-1), as well as their signaling molecules, have been identified during the process of skeletal repair and regeneration. These BMPs are induced by stimuli such as the impact of fracture and mechanical stress just at the regions undergoing the formation of skeletal tissues. The BMPs have also been identified in several pathological skeletal disorders showing the formation of bone and cartilage. In particular, BMP-2 and -4 may act as mediators of early skeletal repair and regenerative reactions, and CDMP-1 may play rather distinct roles, such as the promotion of chondrogenesis and tendon repair.

Such information regarding the involvement of BMPs in skeletal repair and regeneration, together with the actions of BMPs shown by in vivo and in vitro studies, holds the key to the formulation of new strategies for the development of BMP-based orthopedic treatment systems. The possible roles of BMPs in both physiological and pathological conditions provide evidence for the possible application of BMP technology in orthopedic medicine, and indicate a pathway for new advanced approaches in the treatment of orthopedic disorders.

References

1. Urist MR (1965) Bone: formation by autoinduction. Science 150: 893–899
2. Urist MR, Strates BS (1971) Bone morphogenetic protein. J Dent Res 50:1392–1406
3. Wozney JM, Rosen V, Celeste AJ, Mitsock LM, Whitters MJ, Kriz RW, Hewick RM, Wang EA (1988) Novel regulators of bone formation: molecular clones and activities. Science 242:1528–1534
4. Takaoka K, Yoshikawa H, Hashimoto J, Miyamoto S, Masuhara K, Nakahara H, Matsui M, Ono K (1993) Purification and characterization of a bone-inducing protein from a murine osteosarcoma (Dunn type). Clin Orthop 292:329–336
5. Takaoka K, Yoshikawa H, Hasimoto J, Masuhara K, Miyamoto S, Suzuki S, Ono K, Matsui M, Oikawa S, Tsuruoka N, Tawaragi Y, Inuzuka C, Kitayama T, Sugiyama M, Tsujimoto M, Nakanishi T, Nakazato H (1993) Gene cloning and expression of a bone morphogenetic protein derived from a murine osteosarcoma. Clin Orthop 294:344–352
6. Reddi AH (2005) BMPs: from bone morphogenetic proteins to body morphogenetic proteins. Cytokine Growth Factor Rev 16: 249–250
7. ten Dijke P, Yamashita H, Sampath TK, Reddi AH, Estevez M, Riddle DL, Ichijo H, Heldin CH, Miyazono K (1994) Identification of type I receptors for osteogenic protein-1 and bone morphogenetic protein-4. J Biol Chem 269:16985–16988
8. Rosenzweig BL, Imamura T, Okadome T, Cox GN, Yamashita H, ten DP, Heldin CH, Miyazono K (1995) Cloning and characterization of a human type II receptor for bone morphogenetic proteins. Proc Natl Acad Sci U S A 92:7632–7636
9. Zou H, Wieser R, Massague J, Niswander L (1997) Distinct roles of type I bone morphogenetic protein receptors in the formation and differentiation of cartilage. Genes Dev 11:2191–2203
10. Heldin CH, Miyazono K, ten Dijke P (1997) TGF-beta signalling from cell membrane to nucleus through SMAD proteins. Nature 390:465–471
11. Tsumaki N, Tanaka K, Arikawa-Hirasawa E, Nakase T, Kimura T, Thomas JT, Ochi T, Luyten FP, Yamada Y (1999) Role of CDMP-1 in skeletal morphogenesis: promotion of mesenchymal cell recruitment and chondrocyte differentiation. J Cell Biol 144:161–173
12. Wolfman NM, Hattersley G, Cox K, Celeste AJ, Nelson R, Yamaji N, Dube JL, DiBlasio-Smith E, Nove J, Song JJ, Wozney JM, Rosen V (1997) Ectopic induction of tendon and ligament in rats by growth and differentiation factors 5, 6, and 7, members of the TGF-beta gene family. J Clin Invest 100:321–330
13. Friedlaender GE, Perry CR, Cole JD, Cook SD, Cierny G, Muschler GF, Zych GA, Calhoun JH, LaForte AJ, Yin S (2001)

Osteogenic protein-1 (bone morphogenetic protein-7) in the treatment of tibial nonunions. J Bone Joint Surg Am 83-A (Suppl 1):S151–158
14. Govender S, Csimma C, Genant HK, Valentin-Opran A, Amit Y, et al. (2002) Recombinant human bone morphogenetic protein-2 for treatment of open tibial fractures: a prospective, controlled, randomized study of 450 patients. J Bone Joint Surg Am 84-A:2123–2134
15. Nakase T, Nomura S, Yoshikawa H, Hashimoto J, Hirota S, Kitamura Y, Oikawa S, Ono K, Takaoka K (1994) Transient and localized expression of bone morphogenetic protein 4 messenger RNA during fracture healing. J Bone Miner Res 9:651–659
16. Nakase T, Takaoka K, Mizuno S, Hirota S, Sato M, Yoshikawa H, Nomura S (1996) Expression of bone morphogenetic protein-4 mRNA during the process of bone formation in embryogenesis and fracture repair. Wound Repair and Regeneration (Wound Rep Reg) 4:82–86
17. Onishi T, Ishidou Y, Nagamine T, Yone K, Imamura T, Kato M, Sampath TK, ten Dijke P, Sakou T (1998) Distinct and overlapping patterns of localization of bone morphogenetic protein (BMP) family members and a BMP type II receptor during fracture healing in rats. Bone 22:605–612
18. Bostrom MP, Lane JM, Berberian WS, Missri AA, Tomin E, Weiland A, Doty SB, Glaser D, Rosen VM (1995) Immunolocalization and expression of bone morphogenetic proteins 2 and 4 in fracture healing. J Orthop Res 13:357–367
19. Meyer RA Jr, Meyer MH, Tenholder M, Wondracek S, Wasserman R, Garges P (2003) Gene expression in older rats with delayed union of femoral fractures. J Bone Joint Surg Am 85-A:1243–1254
20. Ishidou Y, Kitajima I, Obama H, Maruyama I, Murata F, Imamura T, Yamada N, ten Dijke P, Miyazono K, Sakou T (1995) Enhanced expression of type I receptors for bone morphogenetic proteins during bone formation. J Bone Miner Res 10:1651–1659
21. Rundle CH, Miyakoshi N, Kasukawa Y, Chen ST, Sheng MH, Wergedal JE, Lau KH, Baylink DJ (2003) In vivo bone formation in fracture repair induced by direct retroviral-based gene therapy with bone morphogenetic protein-4. Bone 32:591–601
22. Spinella-Jaegle S, Rawadi G, Kawai S, Gallea S, Faucheu C, Mollat P, Courtois B, Bergaud B, Ramez V, Blanchet AM, Adolphe M, Baron R, Roman-Roman S (2001) Sonic hedgehog increases the commitment of pluripotent mesenchymal cells into the osteoblastic lineage and abolishes adipocytic differentiation. J Cell Sci 114:2085–2094
23. Murtaugh LC, Chyung JH, Lassar AB (1999) Sonic hedgehog promotes somitic chondrogenesis by altering the cellular response to BMP signaling. Genes Dev 13:225–237
24. Miyaji T, Nakase T, Iwasaki M, Kuriyama K, Tamai N, Higuchi C, Myoui A, Tomita T, Yoshikawa H (2003) Expression and distribution of transcripts for sonic hedgehog in the early phase of fracture repair. Histochem Cell Biol 119:253–257
25. Imai Y, Terai H, Nomura-Furuwatari C, Mizuno S, Matsumoto K, Nakamura T, Takaoka K (2005) Hepatocyte growth factor contributes to fracture repair by upregulating the expression of BMP receptors. J Bone Miner Res 20:1723–1730; Epub 2005 June 1720
26. Yoshimura Y, Nomura S, Kawasaki S, Tsutsuminoto T, Shimizu T, Takaoka K (2001) Colocalization of noggin and bone morphogenetic protein-4 during fracture healing. J Bone Miner Res 16:876–884
27. Tsumaki N, Nakase T, Miyaji T, Kakiuchi M, Kimura T, Ochi T, Yoshikawa H (2002) Bone morphogenetic protein signals are required for cartilage formation and differently regulate joint development during skeletogenesis. J Bone Miner Res 17:898–906
28. Kloen P, Doty SB, Gordon E, Rubel IF, Goumans MJ, Helfet DL (2002) Expression and activation of the BMP-signaling components in human fracture nonunions. J Bone Joint Surg Am 84-A:1909–1918
29. Kloen P, Di Paola M, Borens O, Richmond J, Perino G, Helfet DL, Goumans MJ (2003) BMP signaling components are expressed in human fracture callus. Bone 33:362–371
30. Nakase T, Sugamoto K, Miyamoto T, Tsumaki N, Tuyten FP, Inui H, Myoui A, Tomita T, Yoshikawa H (2003) Activation of cartilage-derived morphogenetic protein-1 in torn rotator cuff. Clin Orthop 399:140–145
31. Mikic B, Schalet BJ, Clark RT, Gaschen V, Hunziker EB (2001) GDF-5 deficiency in mice alters the ultrastructure, mechanical properties and composition of the Achilles tendon. J Orthop Res 19:365–371
32. Chhabra A, Tsou D, Clark RT, Gaschen V, Hunziker EB, Mikic B (2003) GDF-5 deficiency in mice delays Achilles tendon healing. J Orthop Res 21:826–835
33. Aspenberg P, Forslund C (1999) Enhanced tendon healing with GDF 5 and 6. Acta Orthop Scand 70:51–54
34. Ilizarov GA (1990) Clinical application of the tension-stress effect for limb lengthening. Clin Orthop 250:8–26
35. Sato M, Ochi T, Nakase T, Hirota S, Kitamura Y, Nomura S, Yasui N (1999) Mechanical tension-stress induces expression of bone morphogenetic protein (BMP)-2 and BMP-4, but not BMP-6, BMP-7, and GDF-5 mRNA, during distraction osteogenesis. J Bone Miner Res 14:1084–1095
36. Testini WT, Wiesel SW (1989) The pathogenesis of cervical spondylosis. Clin Orthop 239:69–93
37. Miyamoto S, Yonenobu K, Ono K (1991) Experimental cervical spondylosis in the mouse. Spine 16:S495–500
38. Nakase T, Ariga K, Miyamoto S, Okuda S, Tomita T, Iwasaki M, Yonenobu K, Yoshikawa H (2001) Distribution of genes for bone morphogenetic protein-4, -6, growth differentiation factor-5, and bone morphogenetic protein receptors in the process of experimental spondylosis in mice. J Neurosurg Spine 94:68–75
39. Inamasu J, Guiot BH, Sachs DC (2006) Ossification of the posterior longitudinal ligament: an update on its biology, epidemiology, and natural history. Neurosurgery 58:1027–1039; discussion 1027–1039
40. Hayashi K, Ishidou Y, Yonemori K, Nagamine T, Origuchi N, Maeda S, Imamura T, Kato M, Yoshida H, Sampath TK, ten Dijke P, Sakou T (1997) Expression and localization of bone morphogenetic proteins (BMPs) and BMP receptors in ossification of the ligamentum flavum. Bone 21:23–30
41. Kawaguchi H, Kurokawa T, Hoshino Y, Kawabara H, Ogata E, Matsumoto T (1992) Immunohistochemical demonstration of bone morphogenetic protein-2 and transforming growth factor-beta in the ossification of the posterior longitudinal ligament of the cervical spine. Spine 17:S33–36
42. Ono M, Russell WJ, Kudo S, Kuroiwa Y, Takamori M, Motomura S, Murakami J (1982) Ossification of the thoracic posterior longitudinal ligament in a fixed population. Radiological and neurological manifestations. Radiology 143:469–474
43. Yanagi T (1997) Clinical manifestation of thoracic ossification of the posterior longitudinal ligament and ossification of the yellow ligament. In: Yonenobu K, Sakou T, Ono K (eds) OPLL: Ossification of the Posterior Longitudinal Ligament. Springer-Verlag, Tokyo, pp 95–98
44. Nakase T, Ariga K, Yonenobu K, Tsumaki N, Tuyten F, Mukai Y, Sato I, Yoshikawa H (2001) Activation and localization of cartilage-derived morphogenetic protein-1 at the site of ossification of the ligamentum flavum. Eur Spine J 10:289–294
45. Huvos AG (1991) Solitary osteocartilaginous exostosis (osteochondroma). In: Huvos AG (ed) Bone Tumors: Diagnosis, Treatment and Prognosis, 2nd edn. W.B. Saunders, Philadelphia, pp 253–264
46. Nakase T, Myoui A, Shinada K, Kuriyama K, Joyama S, Miyaji T, Tomita T, Yoshikawa H (2001) Involvement of BMP-2 signaling in a cartilage cap in osteochondroma. J Orthop Res 19:1085–1088
47. Yoshikawa H, Nakase T, Myoui A, Ueda T (2004) Bone morphogenetic proteins in bone tumors. J Orthop Sci 9:334–340
48. Okuda S, Myoui A, Nakase T, Wada T, Yonenobu K, Yoshikawa H (2001) Ossification of the ligamentum flavum associated with osteoblastoma: a report of three cases. Skelet Radiol 30:402–406
49. Nakase T, Miyaji T, Tomita T, Kaneko M, Kuriyama K, Myoui A, Sugamoto K, Ochi T, Yoshikawa H (2003) Localization of bone morphogenetic protein-2 in human osteoarthritic cartilage and osteophyte. Osteoarthritis Cartilage 11:278–284

関節リウマチ中下位頸椎病変に対する椎弓形成術――上位頸椎固定例と非固定例での比較*

向井克容
細野　昇
坂浦博伸
藤原桂樹
冨士武史
吉川秀樹**

[別冊整形外科 50：108～112，2006]

はじめに

関節リウマチ（RA）における中下位頸椎病変は上位頸椎病変と比較して頻度が低いものの，軽度のすべりでも重篤な脊髄症を惹起する可能性があり，軽視できない病態である．また，病変が多椎間にわたることも多く，その手術的治療についても上位頸椎と比べ議論の余地が大きい．中下位頸椎病変に対する手術的治療に関する過去の報告では固定術をすすめるものがほとんどであるが[1～3]，固定隣接椎間での不安定性出現の問題や，全頸椎固定による頸椎可動域（ROM）消失が関節機能の低下したRA患者の日常生活動作に及ぼす影響も懸念される．われわれは，比較的軽度なRA中下位頸椎病変に伴う脊髄症に対しては，頸椎椎弓形成術を積極的に行ってきた[4]．しかし，RA頸椎病変は上位頸椎での発生頻度が高く，中下位頸椎のみにリウマチ性変化をきたすことは少ないため[5]，上位頸椎固定と同時にあるいは上位頸椎固定後に中下位頸椎の治療が必要になることも多い．上位頸椎固定が中下位頸椎アライメントや中下位頸椎病変の進行に関与するとの報告[6,7]もあるが，上位頸椎固定が中下位頸椎の手術成績に与える影響については不明である．

本研究の目的はRA中下位頸椎病変に対する椎弓形成術の術後成績を上位頸椎固定例と非固定例で比較し，中下位頸椎病変に対する椎弓形成術に上位頸椎固定が与える影響について検討することである．

Ⅰ．対象および方法

1990～2000年にRA中下位頸椎病変に対して手術的治療を行った79例のうち，インストゥルメントを用いて固定術を行った症例が47例，椎弓形成術を行った症例が32例あった．椎弓形成術を行った32例のうち，1年以上追跡が可能であった30（男性11，女性19）例を対象とした．椎弓形成術は原則的に，①軸椎下亜脱臼が比較的軽度で後弯変形を伴わず，②主症状が脊髄症状であり，強い頸部痛を伴わない症例に対して行われた．手術時年齢は平均63.9（46～82）歳であった．30例全例に3 mm以上の軸椎下亜脱臼を認めた．椎弓形成術単独施行例が18例（L群），上位頸椎固定と椎弓形成術を併用した症例が12例（U群）あった．U群のうち2例は上位頸椎固定術後の中下位頸椎病変に対する椎弓形成術であった．椎弓形成術においては蝶番側の骨溝に骨細片（bone chip）を移植した．上位頸椎の固定範囲はC1-C2固定が6例，O～C2（C3）固定が6例で，これら12例においては脊髄症の責任高位は全例，軸椎下亜脱臼レベルであった．外固定については，椎弓形成術単独例はフィラデルフィアカラーを術後1ヵ月，上位頸椎同時固定例ではハローベストを術後1～2ヵ月使用した．RA病型については術前に越智らの分類に準じ，ムチランス型，非ムチランス型の2型に分類した（L群：ムチランス型8例，非ムチランス型10例，U群：ムチランス型4例，非ムチランス型8例）．各群におけるムチランス型と非ムチランス型の比に有意差はなかった．以上の症例に対し，画像評価および臨床評価を行い，L群とU群のあいだで比較を行った．画像評価は，単純X線前後屈側面像

Key words
RA, laminoplasty, subaxial subluxation, upper cervical fusion

*Comparison of laminoplasty for rheumatoid subaxial lesions with and without upper cervical fusion

**Y. Mukai：住友病院整形外科（〒530-0005 大阪市北区中之島5-3-20；Dept. of Orthop. Surg., Sumitomo Hospital, Osaka）；N. Hosono（部長）：大阪厚生年金病院整形外科；H. Sakaura：大阪大学整形外科；K. Fujiwara（部長）：大阪府立急性期・総合医療センター整形外科；T. Fuji（部長）：大阪厚生年金病院整形外科；H. Yoshikawa（教授）：大阪大学整形外科．

でのすべり椎間数（3 mm 以上），すべり量，C2～C7 間の頸椎 ROM を計測し，側面中間位で C2～C7 間の前弯角を計測した．臨床評価は，術直前，術後 6 ヵ月，最終追跡時における神経症状および頸部痛を Ranawat らの分類[1]で評価し，さらに歩行機能については 0～4（0：支持なしで屋外歩行可能，1：支持があれば屋外歩行可能，2：歩行は屋内のみ，3：移動に車椅子要，4：寝たきり）の 5 段階で評価した．術後経過観察期間は平均 3.5（1～9）年であった．統計分析には x^2検定，paired t 検定，Mann-Whitney U 検定，repeated measure ANOVA を用い，危険率 5%未満を有意差ありとした．

Ⅱ．結　　果

1．画像評価

L 群および U 群における術前すべり椎間数と，もっともすべりが大きい椎間でのすべり量は表 1 のとおりであり，両群間で軸椎下亜脱臼の程度に有意差はなかった．最終追跡時，L 群 6 例（33%），U 群 2 例（17%）においてすべりの増悪を認めた．これら 8 例のうち 6（L 群 4，U 群 2）例はムチランス型 RA であった．頸椎 ROM は，L 群では術前平均 29.0°（6°～63°）から最終追跡時平均 11.1°（0°～31°）に減少し，U 群では術前平均 29.1°（11°～41°）から最終追跡時平均 11.8°（0°～30°）に減少した．すべりの増悪，頸椎 ROM 変化とも両群間に有意差を認めなかった．頸椎自然癒合のため ROM が消失した症例が 5（L 群 3，U 群 2）例あった．C2～C7 間の前弯角は，L 群では術前平均 22.8°（5°～63°）から最終追跡時平均 21.9°（－3°～72°）と変化が少なかったのに対し，U 群では術前平均 19.6°（－4°～42°）から最終追跡時平均 9.2°（－8°～23°）と前弯減少が大きかったが，両群間で統計学的な有意差はなかった．

表 1．各群における術前 RA 病型分類と軸椎下亜脱臼

	L 群（n=18）	U 群（n=12）
非ムチランス型/ムチランス型	10/8	8/4
すべり椎間数　1 椎間	15	7
2 椎間	2	3
3 椎間	1	1
4 椎間		1
すべり量　3～5 mm	15	11
5 mm＜	3	1

2．臨床評価

術前頸部痛は L 群 8（Ranawat 分類 grade 1：3，grade 2：4，grade 3：1）例，U 群 8（grade 1：2，grade 2：6，grade 3：0）例に認めた．これら術前頸部痛を認めた 16 例のうち 10（L 群 4，U 群 6）例で最終追跡時 1 段階以上の疼痛改善が得られたが，残る 6（L 群 4，U 群 2）例は術前と変化がなかった．U 群の 1 例のみに術後疼痛の悪化を認めた．

L 群の術前神経症状は Ranawat 分類 class ⅢA が 8 例，class ⅢB が 10 例であったが，そのうち 15 例において術後 1 段階以上の改善を認め，12 例で最終追跡時まで神経症状の改善が維持されていた．U 群では術前 class ⅢA が 9 例，class ⅢB が 3 例であったが，そのうち 9 例において術後 1 段階以上の改善を認め，8 例で最終追跡時まで神経症状の改善が維持されていた．Ranawat の class 分類の改善が得られなかった症例が L 群，U 群合せて 6（L 群 3，U 群 3）例あったが，そのうち 5（L 群 2，U 群 3）例において 1 段階以上の歩行機能改善が得られていた．経過中，神経症状の再悪化を 5（L 群 3，U 群 2）例に認め，このうち 4 例はムチランス型 RA であった．神経症状の改善・維持に関しては L 群と U 群とで有意差を認めなかった．

Ⅲ．症例提示

症例 1． 47 歳，女（図 1）．非ムチランス型 RA．

垂直亜脱臼に対し O～C3 の固定を施行したが，術後 6 年で C4/C5 レベルでの亜脱臼による脊髄症状が発症したため椎弓形成術を施行した．神経症状は Ranawat 分類では術前 classⅢA から術後 classⅢA と変化しなかったが，歩行機能については 1 段階の改善が得られ，術後 3 年の最終追跡時まで維持されていた．X 線像上，最終追跡時には C4/C5 椎体間は自然癒合して安定化し，アライメントの悪化やほかのレベルでの亜脱臼の進行も認めない．

症例 2． 66 歳，男（図 2）．非ムチランス型 RA．

環軸椎前方亜脱臼と C3/C4，C4/C5 レベルでの亜脱臼を認め，軸椎下亜脱臼による脊髄障害を呈していた．Magerl 法による環軸椎固定と椎弓形成術を同時に施行し，神経症状は術前 classⅢA から術後 classⅡに改善し，術後 3 年の最終追跡時まで神経症状の改善は維持されていた．最終追跡時における X 線像では，術前と比較してアライメントに変化はなく，軸椎下亜脱臼の進行も認めない．

Ⅳ．考　　察

RA 中下位頸椎病変は滑膜炎および靱帯付着部炎によ

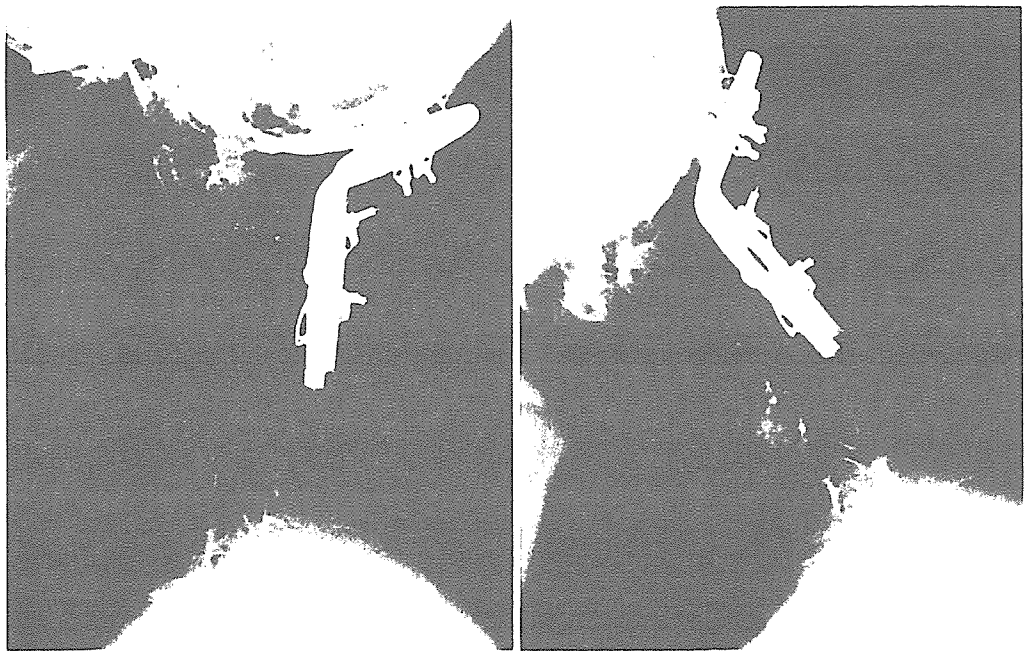

a．椎弓形成術前中間位　　b．椎弓形成術前前屈位

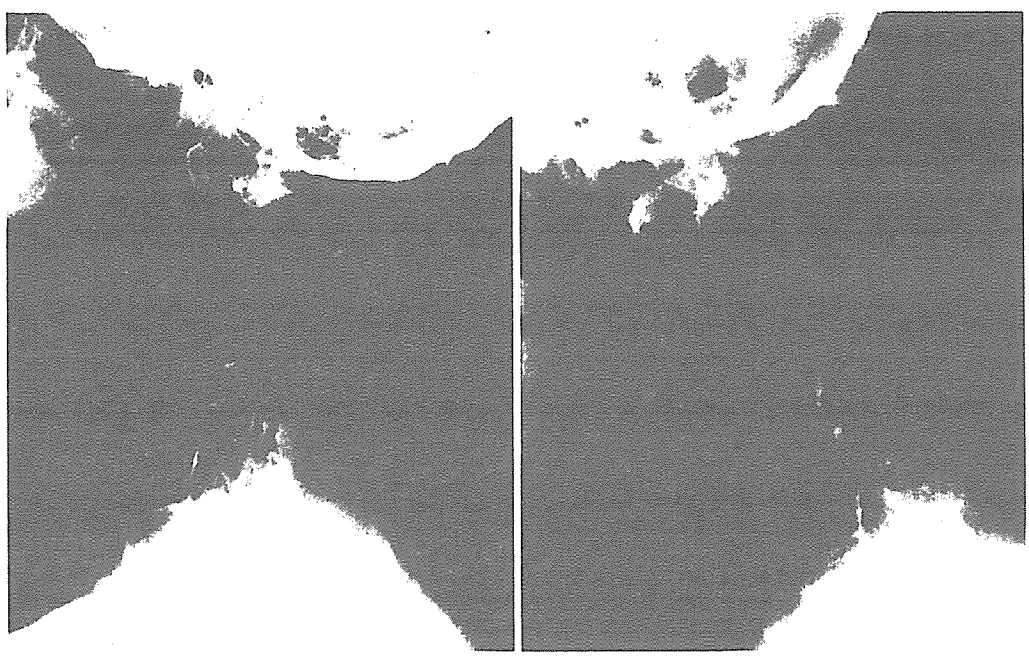

c．術後3年中間位　　d．術後3年前屈位

図1．症例1．47歳，女．非ムチランス型RA．X線像

り，①椎間関節の破壊，②黄色靱帯の炎症性肥厚および椎弓の破壊，③棘突起の侵食・菲薄化，④棘上・棘間靱帯の機能不全および断裂，⑤椎間板・椎体終板の破壊などの変化で脊椎支持組織が全周性に破綻して亜脱臼をきたし，さらに脊柱管の発育性狭窄や脊柱管内リウマチ性肉芽形成なども相まって圧迫性脊髄障害をきたす病態である．RA中下位頚椎病変治療についての過去の報告は固定術に関するものがほとんどであり[1~3]，その治療においては強固な固定が不可欠と一般的に考えられてきた．したがって，椎弓形成術が中下位頚椎病変に対して行われることは少なく，中下位頚椎病変に対する椎弓形成術を詳細に検討した報告もきわめて少ない[4,7]．

われわれは以前から，比較的軽度な中下位頚椎病変による脊髄症に対しては，内固定材料を用いた固定術と比べて簡便で侵襲も少ない椎弓形成術を積極的に行ってきた．比較的軽度な中下位頚椎病変による脊髄症に対しては，非ム

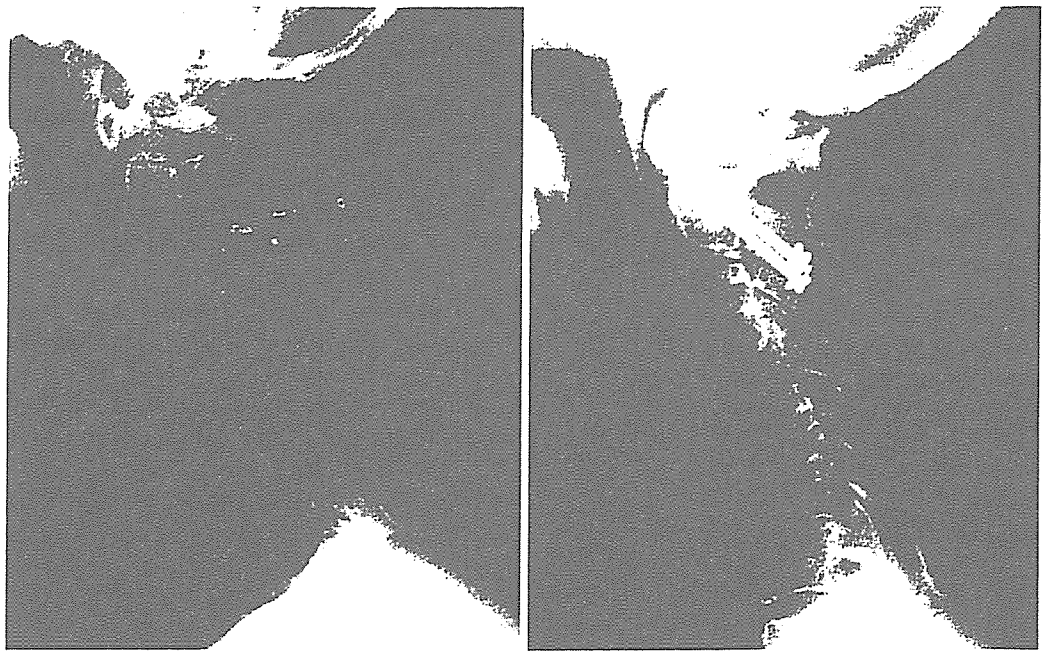

a．術前中間位　　b．術後3年中間位

図2．症例2．66歳，男．非ムチランス型RA．X線像

チランス型である限り椎弓形成術で良好な成績が期待できるが，ムチランス型の場合にはたとえ術前の頸椎病変が軽度であっても，成績不良であることをすでに報告している[4]．中下位頸椎病変には上位頸椎の不安定性を合併する症例も多く，上位頸椎固定の併用を必要とする場面にしばしば遭遇する．上位頸椎固定のさいには軸椎から頸部伸筋群を剝離する必要があり，後方支持組織が脆弱なRA頸椎においては筋剝離による影響も考慮する必要があろう．上位頸椎固定が中下位頸椎アライメントや中下位頸椎病変の進行に影響を与えるとの報告もあり[8]，上位頸椎固定を行った場合には中下位頸椎病変に対する手術は内固定材料を併用した強固な固定を行わないと，アライメントやすべりの悪化を生じるのではないかとの懸念があった．

今回の検討では，L群とU群との比較ですべりの増悪や頸椎ROM変化に有意差はなく，上位頸椎固定が椎弓形成術後の不安定性増悪因子とはなっていなかった．また頸椎アライメントに関しては，統計学的有意差はなかったもののL群よりU群のほうが術後前弯減少が強かった．一方，神経症状の改善・維持については両群間で有意差はなく，U群における前弯減少は神経症状に影響を与えるほどのものではなかったといえる．すべり増悪例の75%，神経症状再悪化例の80%はムチランス型RAであり，成績不良因子としては上位頸椎固定の有無ではなく，RA重症度が関与していた．頸椎ROMが消失していた症例があったが，蝶番側の骨溝への骨細片移植がROM消失にどの程度関与しているかは不明である．骨癒合は骨移植部以外の椎弓間や椎体間などにさまざまな程度で自然癒合として認められたが，骨癒合の発生部位，発生範囲，癒合隣接椎間での変化に一定の傾向はみられなかった．蝶番側への骨移植が必要か否かについては今後の検討を要するが，ムチランス型以外のほとんどの症例ではX線像上の安定性と日常生活に支障がない程度のROM温存の両者を獲得できた．頸部痛に関しては，U群のほうが疼痛改善がよい傾向にあったが，これは頸部痛の原因として上位頸椎での不安定性の関与が大きいため，上位頸椎固定により疼痛の改善が得られたことが原因と考えられる．またL群で頸部痛が改善しなかった4例中3例は，術前頸部痛がgrade 1の軽い頸部痛であった．

上位頸椎不安定性と中下位頸椎病変による脊髄症が並存する場合に，中下位頸椎にどのような術式を選択しうるのかについてはこれまで報告がなかった．自験例における術前軸椎下亜脱臼は，大半の症例において5 mm以下，2椎間までであり，この程度のすべりであれば非ムチランス型である限り上位頸椎固定を併用しても椎弓形成術で良好な成績が期待できる．

まとめ

1）RA中下位頸椎病変に対する椎弓形成術の成績を，椎弓形成術単独群と上位頸椎固定併用群で比較し，上位頸椎

固定が椎弓形成術の成績に与える影響について検討した.

2) 上位頚椎固定群では椎弓形成術単独群と比べて, すべりの増悪, ROM 変化, 前弯減少などの X 線変化に統計学的有意差はなく, また神経症状の改善・維持に関しても両群間で有意差を認めなかった.

3) 比較的軽度な中下位頚椎病変に対しては, 非ムチランス型である限り上位頚椎固定を併用しても椎弓形成術で良好な成績が期待できる.

文 献

1) Ranawat CS, O'Leary P, Pellici P et al : Cervical spine fusion in rheumatoid arthritis. J Bone Joint Surg **61**-A : 1003-1010, 1979
2) Santavirta S, Konttinen YT, Sandelin J et al : Operations for the unstable cervical spine in rheumatoid arthritis ; sixteen cases of subaxial subluxation. Acta Orthop Scand **61** : 106-110, 1990
3) Olerud C, Larsson BE, Rodriguez M : Subaxial cervical spine subluxation in rheumatoid arthritis. Acta Orthop Scand **68** : 109-115, 1997
4) Mukai Y, Hososno N, Sakaura S et al : Laminoplasty for cervical myelopathy caused by subaxial lesions in rheumatoid arthritis. J Neurosurg **100** : 7-12, 2004
5) Fujiwara K, Owaki H, Fujimoto M et al : A long-term follow-up study of cervical lesions in rheumatoid arthritis. J Spinal Disord **13** : 519-526, 2000
6) Yoshimoto H, Ito M, Abumi K et al : A retrospective radiographic analysis of subaxial sagittal alignment after posterior C1-C2 fusion. Spine **29** : 175-181, 2004
7) Suda Y, Saitou M, Shioda M et al : Cervical laminoplasty for subaxial lesion in rheumatoid arthritis. J Spinal Disord Tech **17** : 94-101, 2004
8) Matsunaga S, Onishi T, Sakou T : Significance of occipitoaxial angle in subaxial lesion after occipitocervical fusion. Spine **26** : 161-165, 2001

* * *

DOI: 10.1534/genetics.105.048934

A Novel Murine Gene, *Sickle tail*, Linked to the *Danforth's short tail* Locus, Is Required for Normal Development of the Intervertebral Disc

Kei Semba,*,† Kimi Araki,* Zhengzhe Li,* Ken-ichirou Matsumoto,*,† Misao Suzuki,‡ Naoki Nakagata,§ Katsumasa Takagi,† Motohiro Takeya, Kumiko Yoshinobu,†† Masatake Araki,†† Kenji Imai,‡‡ Kuniya Abe§§ and Ken-ichi Yamamura*,1**

**Division of Developmental Genetics, Institute of Molecular Embryology and Genetics, Kumamoto University, Kumamoto 862-0976, Japan, †Department of Orthopaedic Surgery, Kumamoto University School of Medicine, Kumamoto 860-8556, Japan, ‡Division of Transgenic Technology, Institute of Resource Development and Analysis, Kumamoto University, Kumamoto 860-0811, Japan, §Division of Reproductive Engineering, Institute of Resource Development and Analysis, Kumamoto University, Kumamoto 860-0811, Japan, **Department of Cell Pathology, Kumamoto University School of Medicine, Kumamoto 860-8556, Japan, ††Division of Bioinformatics, Institute of Resource Development and Analysis, Kumamoto University, Kumamoto 860-0811, Japan, ‡‡Institute of Developmental Genetics, GSF-National Research Center for Environment and Health, 85764 Neuherberg, Germany and §§Technology Development Team for Mammalian Cellular Dynamics, BioResource Center, RIKEN, Tsukuba, Ibaraki 305-0074 Japan*

Manuscript received July 29, 2005
Accepted for publication September 26, 2005

ABSTRACT

We established the mutant mouse line, B6;CB-*Skt*$^{Gt(Ayu802)HMEG}$ (*Skt*^{Gt}), through gene-trap mutagenesis in embryonic stem cells. The novel gene identified, called *Sickle tail* (*Skt*), is composed of 19 exons and encodes a protein of 1352 amino acids. Expression of a reporter gene was detected in the notochord during embryogenesis and in the nucleus pulposus of mice. Compression of some of the nuclei pulposi in the intervertebral discs (IVDs) appeared at embryonic day (E) 17.5, resulting in a kinky-tail phenotype showing defects in the nucleus pulposus and annulus fibrosus of IVDs in *Skt*$^{Gt/Gt}$ mice. These phenotypes were different from those in *Danforth's short tail* (*Sd*) mice in which the nucleus pulposus was totally absent and replaced by peripheral fibers similar to those seen in the annulus fibrosus in all IVDs. The *Skt* gene maps to the proximal part of mouse chromosome 2, near the *Sd* locus. The genetic distance between them was 0.95 cM. The number of vertebrae in both [*Sd* +/+ *Skt*^{Gt}] and [*Sd Skt*^{Gt}/+ +] compound heterozygotes was less than that of *Sd* heterozygotes. Furthermore, the enhancer trap locus *Etl4*^{lacZ}, which was previously reported to be an allele of *Sd*, was located in the third intron of the *Skt* gene.

THE notochord is an integral component of the axial structure of vertebrates, functions as a signaling center during embryogenesis, and plays essential roles in patterning of both somites and the neural tube (Ang and Rossant 1994; Wilson *et al.*1995; Chiang *et al.*1996). In addition, the notochord has major roles in vertebral column formation. In the mouse, the notochord is a continuous rod of constant diameter extending from the hypophysis to almost the tip of the tail at embryonic day (E) 9.5. At E10.5–E11.5, signals from the notochord induce the migration, proliferation, and fusion of the sclerotome to form a continuous and unsegmented perichordal tube around the notochord and neural tube. At 12.5, mesenchyme acquires a characteristic metameric pattern of densely packed areas caudally and loosely packed areas cranially. Some densely packed cells move cranially and give rise to the annulus fibrosus of the future intervertebral disc (IVD). The remaining densely packed cells fuse with the immediately caudal loosely packed cells to form the cartilaginous primordia of the vertebral bodies. Notochord cells located in the vertebral body of cranial regions start to relocate into intervertebral regions (Paavola *et al.* 1980; Rufai *et al.* 1995; Aszodi *et al.* 1998). At E13.5, the vertebral regions are enlarged and chondrified. The notochord proliferates and undergoes hypertrophy to form the gelatinous center of the intervertebral disc, called the nucleus pulposus. This nucleus is surrounded by the circularly arranged fibers of the annulus fibrosus. These two structures together constitute the IVD (Langman 1969; Theiler 1988). At E14.5, nearly all chondrocytes are hypertrophied. Starting from E14.5, the annulus fibrosus can be subdivided into a fibrous outer annulus and a cartilaginous inner annulus. At E16.0, notochord cells complete relocation from vertebral regions into

Sequence data from this article have been deposited with the EMBL/GenBank Data Libraries under accession nos. AB125594, AB125595, and AB033043.

[1]*Corresponding author:* Division of Developmental Genetics, Institute of Molecular Embryology and Genetics, Kumamoto University, 4-24-1 Kuhonji, Kumamoto 862-0976, Japan.
E-mail: yamamura@gpo.kumamoto-u.ac.jp

intervertebral regions. Failures in somite, neural tube, and notochord formation are closely correlated with vertebral malformations. However, the mechanisms that underlie the formation of IVDs are largely unknown.

In the mouse, several mutations are known to affect the formation of the vertebral column due to functional defects in the notochord, including *Danforth's short tail* (*Sd*) and the enhancer trap line ($Etl4^{lacZ}$). *Sd*, located on chromosome 2 (LANE and BIRKENMEISER 1993; ALFRED *et al.* 1997), is a semidominant mutation affecting the development of the vertebral column and the urogenital system (DUNN *et al.* 1940; GRUNEBERG 1953, 1958). At E9.5, the notochord shows discontinuities. At E11.5, mesenchymal organization around the notochord is abnormal. At E13.5, the notochord is fragmented and does not show proliferation and dilatation. Chondrification is much reduced in vertebral regions. Thus, an early reduction of the notochord results in cellular degeneration in the sclerotome, leading to reduced vertebral bodies and a characteristic short tail due to a reduced number of caudal vertebrae. Homozygous *Sd* animals show a similar but much more severe tailless phenotype. In the enhancer trap line, $Etl4^{lacZ}$, a reporter (*lacZ*) gene was inserted near the *Sd* locus and was expressed in the notochord, mesonephric mesenchyme, and apical ectoderm ridge (GOSSLER *et al.* 1989; KORN *et al.* 1992; MAATMAN *et al.* 1997; ZACHGO *et al.* 1998). $Etl4^{lacZ}$ homozygotes exhibited kinks in the caudal region of their tails and a synergistic genetic interaction between $Etl4^{lacZ}$ and *Sd* was observed. Genetically, $Etl4^{lacZ}$ and *Sd* are separated by 0.75 cM. Interestingly, attenuation or enhancement of the *Sd* phenotype was observed when the $Etl4^{lacZ}$ insertion was in a *cis*- or *trans*-conformation, respectively. This suggests that $Etl4^{lacZ}$ is an allele of *Sd*, presumably by trapping a *cis*-regulatory element of the *Sd* gene, and that *Sd* is a gain-of-function mutation (ZACHGO *et al.* 1998). Nevertheless, neither the *cis*-element nor the trapped gene has been identified.

In this study, we report a new mutant mouse line, Skt^{Gt}, obtained by gene-trap mutagenesis in embryonic stem (ES) cells. $Skt^{Gt/Gt}$ mice exhibit a kinky tail in the caudal vertebral columns due to malformation of the IVDs. The gene identified, *Sickle tail* (*Skt*), was expressed in the notochord, its derivative nucleus pulposus, and in the mesonephros. Interestingly, the *Skt* gene maps to the proximal part of mouse chromosome 2, near the locus for *Sd*, and the *lacZ* insertion site in $Etl4^{lacZ}$ was found to be located in the third intron of the *Skt* gene. Furthermore, a cumulative effect of the Skt^{Gt} mutation on the *Sd* mutant was observed.

MATERIALS AND METHODS

Generation and genotyping of mutant mice: The gene-trap method using the pU-8 trap vector was previously described (ARAKI *et al.* 1999). Chimeric mice were produced by the aggregation method using ES gene-trap clones and morulas of ICR (Charles River, Wilmington, MA) mice, and the chimeric mice were mated with C57BL/6 (CLEA) females to obtain F_1 heterozygotes. *Sd* mice were purchased from the Jackson Laboratory (Bar Harbor, ME) and propagated by *in vitro* fertilization. *Sd* +/+ Skt^{Gt} mice were generated by mating *Sd* +/+ + mice (C57BL/6 genetic background) to $Skt^{Gt/Gt}$ mice with a C57BL/6 genetic background. One heterozygote carrying the *Sd* mutation and the Skt^{Gt} insertion on the same chromosome (*Sd* Skt^{Gt}/+ +; *cis*-configuration) was obtained through mating between *trans*-heterozygotes and wild-type C57BL/6 mice. *Sd* mice were distinguished by external inspection. Genotyping for Skt^{Gt} alleles was done with PCR using tail genomic DNA as a template. For the wild-type allele, the 5′ primer, GTS (5′-CCACCCCTACATGTGTCTTT-3′), and the 3′ primer, GTA (5′-CGAGTAAGTAACATCCCTCC-3′) located in the 14th intron, were used to generate a 339-bp wild-type fragment. To detect the trapped allele, the 5′ primer, called Z1 (5′-GCGTT ACCCAACTTAATCG-3′), and the Z2 (5′-TGTGAGCGAGTAA CAACCCG-3′) located in *lacZ* gene, were used to generate a 320-bp fragment.

Skeletal preparations: After tail skins were peeled off, tails were fixed in 95% ethanol for 3 days. Tails were cleared by placing in 1% KOH for 1 day and were stained in alizarin red for 1 day until the bone was red. Excess stain was removed with 2% KOH. After removing excessive alizarin red stain, tails were transferred to glycerol (HOGAN *et al.* 1994).

To count the number of vertebral bodies, we examined all mice by X-ray photography. We counted the number of normal vertebral bodies, that is, those without obvious malformations, but did not consider the size reduction observed in the vertebral bodies of *Sd* mutants.

Cloning of genomic DNA and cDNA: Plasmid rescue to obtain flanking genomic DNA was performed as described (ARAKI *et al.* 1999). The 5′-end of the cDNA of the trapped gene was isolated by 5′-rapid amplification of cDNA ends (5′-RACE) using the 5′-RACE system (Invitrogen, Carlsbad, CA). Total RNA from a B6;CB-$Skt^{GtAyu8021IMEG}$ gene-trapped ES clone was extracted by using Sepasol-RNA I (NACALAI TESQUE, Kyoto, Japan), and then poly(A)+ RNA was isolated with an oligo(dT) column (Takara Biomedicals, Shiga, Japan). First-strand cDNA synthesis from 1 μg of poly(A)+ RNA was performed with reverse transcriptase from ReverScript (Wako, Osaka, Japan) and with the primer SA13 (5′-TCTGAAACT CAGCCTTGAGC-3′) in the splice acceptor (SA) sequence. After dCTP tailing with terminal deoxynucleotidyl transferase (Invitrogen), cDNA was purified using a QIAquick nucleotide removal kit (QIAGEN, Chatsworth, CA). The initial PCR was performed using the primer SA10 (5′-AGCAGTGAAGGCTGT GCGA-3′) in the SA sequence and the anchor primer (5′-GGCCACGCGTCGACTAGTACGGGiiGGGiiGGGiiG-3′) (Invitrogen). Then, nested PCR was performed using primer 63 (5′-GCTTGTCCTCTTTGTTAGGG-3′) in the SA sequence and the amplification primer (5′-GGCCACGCGTCGACTAGTAC-3′) in the anchor primer sequence. Amplified fragments were then sequenced directly by the dideoxy-chain termination method using Big Dye terminator cycle sequencing (Perkin-Elmer, Foster City, CA).

RT–PCR analysis: RT–PCR was performed using the Thermoscript RT–PCR system (Invitrogen) according to the manufacturer's instructions. The PCR was performed using the primers a–f in the sense and antisense sequences in the *Skt* gene. The sequences of the primers used are as follows: primer-a, 5′-TCACCATGAAGATGCTGGAG-3′; primer-b, 5′-CTACAG TAAGCACTCGCTGAC-3′; primer-c, 5′-ACTCCTCAGCCTTG ATGAAC-3′; primer-d, 5′-GTGGTGGTAAGTCCTGATCC-3′; primer-e, 5′-GCCACCTTAAAGACACTAGG-3′; and primer-f, 5′-TGAGGAGGAAGAGGTAGTAG-3′. The PCR conditions were

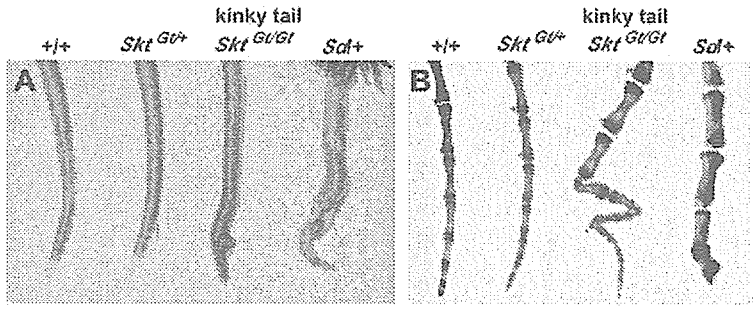

FIGURE 1.—(A) Tail phenotype of 8-week-old mice. $Skt^{Gt/Gt}$ mice had kinked tails compared to wild-type, $Skt^{Gt/+}$, and heterozygous *Sd* mice. (B) Alizarin red whole-mount preparations of the tails of 8-week-old mice. $Skt^{Gt/Gt}$ mice confirmed this kinky-tail phenotype. *Sd* mice showed decreased numbers of vertebrae with truncation at the caudal vertebrae.

94° for 1 min, 55° for 2 min, and 72° for 2 min using 0.5 units of Taq polymerase for 30 cycles.

Northern blot analysis: Total RNA and poly(A)+ mRNA isolated from ES cells and embryo and adult tissues were electrophoresed on a 0.7% denaturing formaldehyde-MOPS-containing agarose gel and transferred to a positively charged nylon membrane (Roche). After baking at 80° for 1 hr, the membrane was prehybridized and then hybridized using the *Skt* gene-specific RNA probes and the *lacZ* RNA probes prepared using DIG RNA labeling and detection kit (Roche).

Detection of β-galactosidase (*lacZ*) activities: Whole-mount X-gal staining was performed according to the method of ALLEN *et al.* (1988). Samples were fixed for 30 min at room temperature in fix solution [1% formaldehyde, 0.2% glutaraldehyde, and 0.02% NP-40 in phosphate-buffered saline (PBS)]. Fixed samples were washed two times in PBS and incubated overnight at 30° in staining solution (5 mM potassium ferricyanide, 5 mM potassium ferrocyanide, 2 mM $MgCl_2$, 0.5% X-gal in PBS). Samples were rinsed twice in PBS, postfixed in 4% paraformaldehyde, and made transparent using benzylalcohol/benzylbenzoate (1:2) after dehydration with a series of ethanol steps (25, 50, 70, 100, and 100%, 1 hr each). Adult tissues were fixed in 4% paraformaldehyde in PBS. Tissue sections of 10 μm were prepared and stained overnight at 30° with X-gal in staining solution. After staining, sections were counterstained with Fast Red. For the section of the intervertebral discs, after X-gal stained tails were refixed in 3.7% formaldehyde/PBS, the caudal vertebral bones were demineralized in Plank–Rychlo solution and embedded in paraffin according to standard procedures. Sections of 8 μm were prepared and counterstained with Nuclear Fast red.

Construction and transfection of the *Skt* expression vector: To clone the full open reading frame (ORF) of the *Skt* gene, RT–PCR was performed using the Thermoscript RT–PCR system. The initial PCR was performed using the primer ORFS1 in the sense strand upstream from the start codon in the *Skt* gene (5′-ACCGGAGTGGAGACTAGTTG-3′) and primer ORFA1 in the antisense strand downstream from the stop codon in the *Skt* gene (5′-TGCATGAGGCCTTGAACGATACAG-3′). Then, nested PCR was performed using the sense-strand primer ORFS2 (5′-TTTCTGCGAGCTTTCCGAAC-3′) and the antisense-strand primer ORFA2 (5′-ACCTTGGTCCTAATAGGATCTG GC-3′). The PCR conditions used were 94° for 1 min, 58° for 1 min, and 72° for 3 min using 1.0 unit of LA Taq polymerase (Takara Biomedicals) for 25 cycles. The 4.1-kb PCR products were cloned into the pGEM-T vector (Promega, Madison, WI). This cDNA ORF was confirmed by sequencing and cloned into the pCAGGS expression vector (NIWA *et al.* 1991). Transfection into BMT10 cells (GERARD and GLUZMAN 1985) was carried out by the lipofection method using LipofectAMINE reagent (Invitrogen).

Western blot analysis: BMT10 cells and 40 pieces of the nucleus pulposus of caudal IVDs of adult mice were homogenized in 2× sample buffer (100 mM Tris HCl pH 6.8, 4% SDS, 12% β-mercaptoethanol, 20% glycerol). Extracts were electrophoresed on a 6.0% polyacrylamide gel, transferred to a nitrocellulose filter (Immobilon, Millipore, Bedford, MA), and detected using anti-Skt antibodies with the ECL detection system (Amersham, Arlington Heights, IL).

Immunohistochemistry: Tails were fixed in 4% paraformaldehyde in PBS. The caudal vertebral bones were demineralized in 0.24 M EDTA·2Na, 0.22 M EDTA·4Na solution for 48 hr and embedded in paraffin blocks. Sections of the IVDs were immunostained with anti-Skt antibodies by the avidin–biotin complex method (Vector Laboratories, Burlingame, CA). Sections were counterstained with hematoxylin.

RESULTS

Generation of *Sickle tail* mutant mice: A gene-trap ES clone was isolated by the exchangeable gene-trap method using the trap vector pU-8 (ARAKI *et al.* 1999). We obtained eight chimeric mice of which three were germline chimeras. Heterozygous animals appeared normal and were fertile. About half (35/66) of the homozygotes, however, showed a peculiar kinky-tail phenotype (Figure 1A and Table 1). This mutant mouse line was designated as B6;CB-$Skt^{Gt(Yu8021IMEG}$, in which *Skt* means *Sickle tail* because of the characteristic shape of the tail. Shortened and curved caudal vertebrae were apparent by the age of 2 weeks and were restricted to the 20–25th caudal vertebrae (Figure 1B). In contrast, heterozygous *Sd* mice showed short tails with truncation of vertebral columns at the 6th caudal vertebral body on average (Figures 1B and 7A) as reported previously. In $Skt^{Gt/Gt}$ mice, no other skeletal abnormality was observed by bone X-ray examination (data not shown).

TABLE 1

Summary of genotyping of 4-week-old mice from Skt^{Gt} heterozygote matings

		Gt/Gt	
+/+	*Gt*/+	Kinked	Normal[a]
60	151	35 (53%)	31

[a] All normal-looking homozygotes showed deformity of the caudal discs by histological analysis.

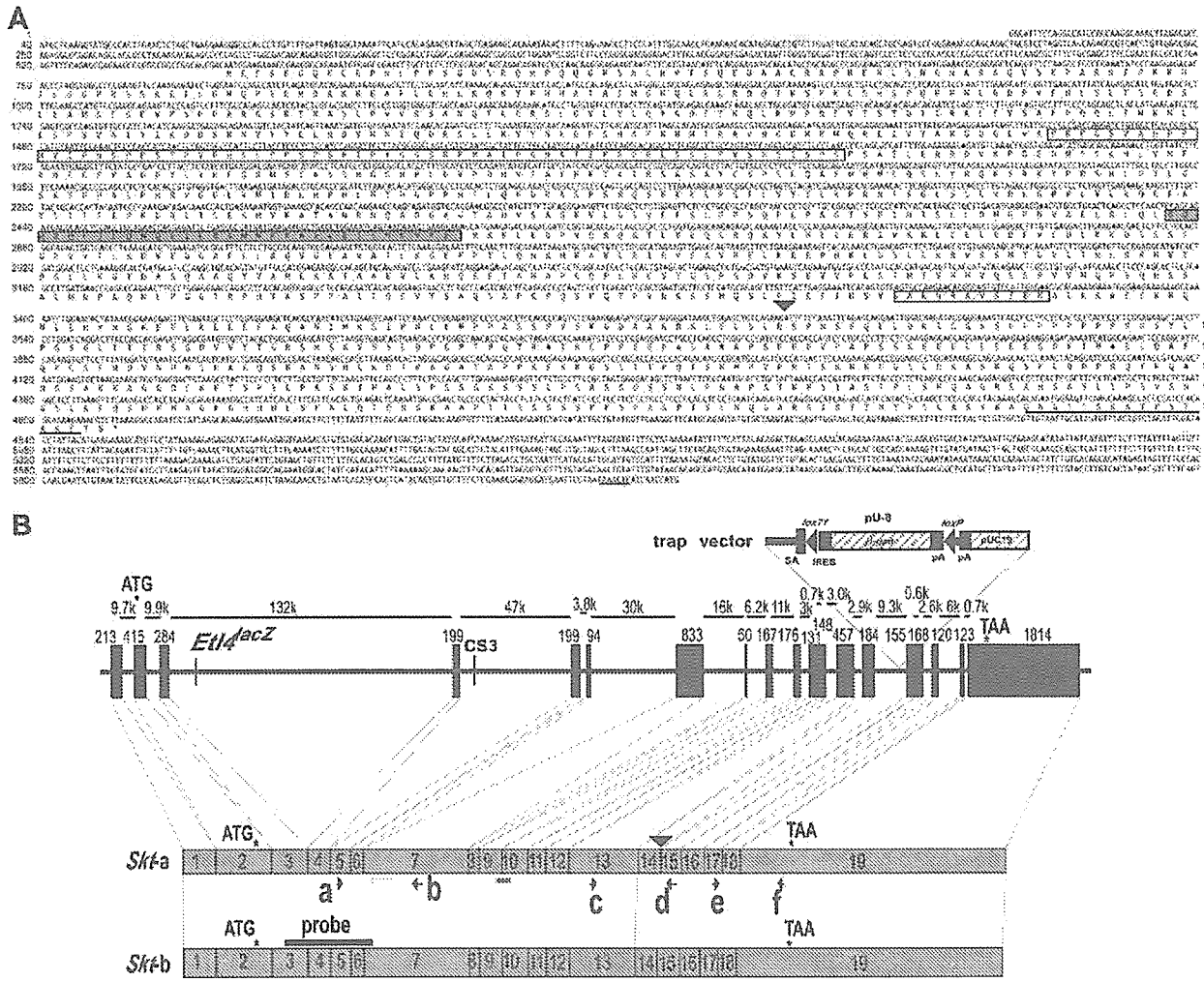

FIGURE 2.—Identification of the trapped gene *Skt*. (A) The nucleotide sequence of the *Skt* cDNA and predicted amino acid sequence. The open box indicates the pro-rich region at the N terminus and the shaded box indicates the coiled-coil region in the middle. The striped box indicates the sequence deleted in *Skt*-b by alternative splicing. The 15-amino-acid peptide used for the production of anti-Skt antibodies is shown by underlining. The polyadenylation signal is underlined at the 3′-end of the nucleotide sequence. The nucleotide sequence is numbered on the left side and the amino acid sequence is numbered on the right side. (B) Genomic structure of the *Skt* gene. (Top) Exon-intron structure of the *Sickle tail* gene. The trap vector, pU-8, was inserted into the 14th intron. Sizes of exons and introns are given. (Bottom) Two transcripts produced from the *Skt* allele. There are at least two types of *Skt* transcripts: one contains all the exons (termed *Skt*-a) and the other lacks 33 bp of the 13th exon (termed *Skt*-b). Arrows (a–f) indicate the location of the primers used for RT–PCR analyses in Figure 3, A–C, to detect the expression of each part of the *Skt* transcripts. The solid bar represents a probe used for Northern blotting. The open and shaded boxes indicate the pro-rich region and the coiled-coil region, respectively. The start and stop codons of the *Skt* gene are shown by asterisks. A sequence with high homology to the CS3 in node/notochord enhancers is located in the fourth intron of the *Skt* gene 106 kb downstream of the insertion site of $Etl4^{lacZ}$.

Characterization of the integration site of the trap vector: To characterize the gene-trap locus, we cloned and sequenced genomic DNA fragments flanking the gene-trap vector. A single copy of the vector was integrated into the genome as determined by Southern blot analysis using genomic DNA samples extracted from Skt^{Gt} mice. Three base pairs of genomic DNA were deleted at the integration site of the trap vector. Using PCR amplification on genomic DNA samples, the genotype of offspring from the heterozygous intercross was easily determined (data not shown).

Identification of the *Sickle tail* gene: To identify the gene trapped, we performed 5′-and 3′-RACE. The sequence of the ORF of the trapped gene was determined by compiling sequences of 5′- and 3′-RACE products and of EST that showed 100% homology to the RACE products. We thus obtained a cDNA sequence comprising 5930 nucleotides (accession no. AB125594) that encodes a putative protein of 1352 amino acids with a predicted molecular weight of 147 kDa (Figure 2A). This gene was termed *Skt*. The protein contains a proline-rich region (amino acid residues 298–364) and a coiled-coil region

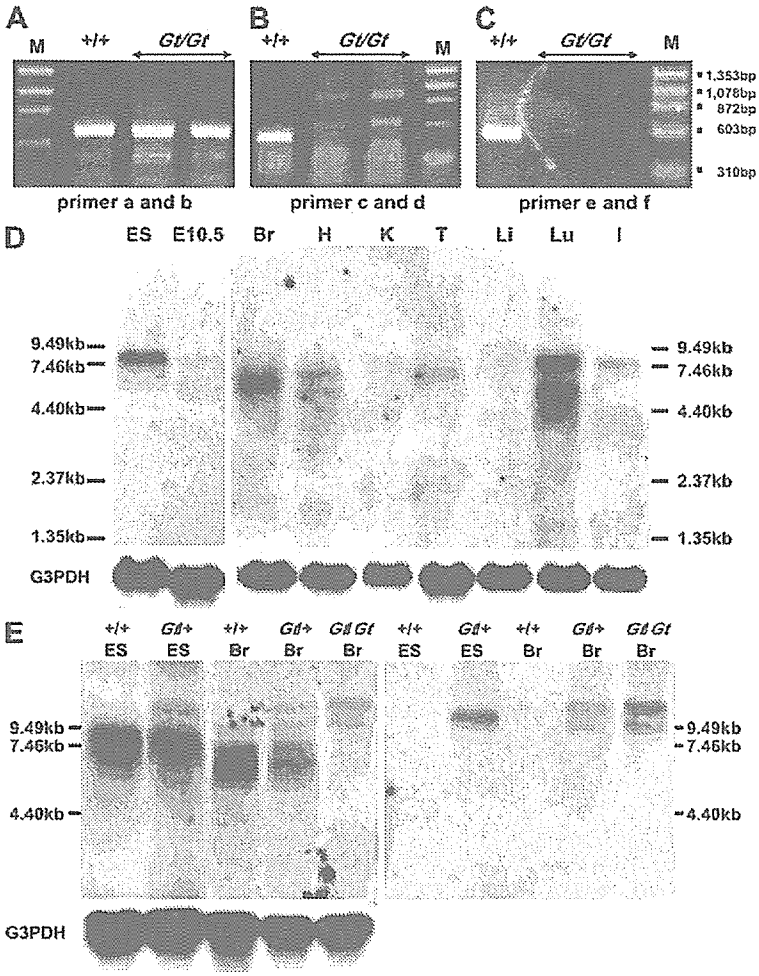

FIGURE 3.—Analyses of *Skt* transcripts. (A–C) RT–PCR analyses using E10.5 embryos to detect *Skt* transcripts in wild-type (+/+) and $Skt^{Gt/Gt}$ embryos. The transcripts containing nucleotide sequences upstream of the insertion site of the trap vector were detected in both wild-type and $Skt^{Gt/Gt}$ embryos (A). The transcripts containing nucleotide sequences downstream of the *Skt* sequence were not detected in $Skt^{Gt/Gt}$ embryos (B and C). M, molecular marker. (D) Northern blot analyses to detect *Skt* mRNA in the wild-type ES cells, E10.5 embryo, and 8-week-old mice, using the *Skt*-specific probe in the 5′-region (see Figure 2B). Total RNA (10 μg) from TT2 ES cells, wild-type E10.5 embryos, mRNA (5 μg) from wild-type organs, and a *Skt* RNA probe were used for Northern blotting. (E) Northern blot analyses to detect *Skt* and β-*geo* fusion transcripts. Total RNA (20 μg) from TT2 and heterozygous (*Gt*/+) ES cells, wild-type (+/+), heterozygous (*Gt*/+), and homozygous (*Gt*/*Gt*) adult brains was used for Northern blotting. The *Skt* RNA probe or *lacZ* RNA probe was used in the left and right panels, respectively. Br, brain; H, heart; K, kidney; T, testis; Li, liver; Lu, lung; I, intestine.

(amino acid residues 626–656) as determined by analysis using Lupas's algorithm (LUPAS *et al.* 1991). An ATG codon is located at nucleotide positions 559–561. This codon is most likely the initiation codon, because there is a Kozak sequence surrounding this ATG codon (KOZAK 1996): *i.e.*, there is a G residue following the ATG codon and an A residue three nucleotides upstream. A BLAST search of the amino acid sequence deduced from the *Skt* cDNA sequence revealed 80.6% homology with an uncharacterized human protein, KIAA 1217 (accession no. AB033043), and no other evolutionarily conserved protein was identified.

Sequence comparison of *Skt* cDNA with the murine genome sequence in the public Mouse Genome Resources (http://www.ncbi.nlm.nih.gov/genome/guide/mouse/) revealed that the *Skt* gene consists of 19 exons spanning >300 kb and that the ATG codon is located in the second exon (Figure 2B). The trap vector was integrated in the 14th intron, resulting in the disruption of the Skt protein at position 998 (arrowhead in Figure 2, A and B). Sequence analyses of fusion transcripts revealed the presence of two fusion transcripts with the β-*geo* sequence: *Skt-a*, containing the 1st–14th exons, and *Skt-b*, lacking 33 bp of the 13th exon from *Skt-a* (Figure 2B). In any case, a truncated protein lacking 355 amino acids encoded by exons 15–19 in the C-terminal region is expected to be produced from the Skt^{Gt} allele.

RT–PCR and Northern blot analyses: We performed RT–PCR using wild-type and $Skt^{Gt/Gt}$ embryos at E10.5. RT–PCR with primers a and b located within the 5′-region of the integration site and detected the expected band in both embryos (Figure 3A). Using RT–PCR with two primer pairs—c in the 5′-region and d in the 3′-region of the integration site and primers e and f within the 3′-region of the integration site—we could not detect any product in $Skt^{Gt/Gt}$ embryos (Figure 3, B and C), indicating the absence of *Skt* mRNA containing exons 15–19 in $Skt^{Gt/Gt}$ embryos.

To analyze the size and expression pattern of *Skt* mRNA, we performed Northern blot analysis using the *Skt*-specific probe in the 5′-region (see Figure 2B). As shown in Figure 3D, a major band of 8 kb and a minor band of 6.5 kb were detected in wild-type ES cells. In wild-type whole embryos at E10.5, the 8- and 6.5-kb bands were also detected, although the expression levels were low. Surprisingly, Northern blot analysis using mRNA

from wild-type adult organs revealed the presence of four different mRNA transcripts, 5.5, 6.5, 7.0, and 8.0 kb. The faint 7.0-kb and strong 6.5-kb bands in the brain, the 7.0- and 5.5-kb bands in the heart, the 7.0-kb band in the testis, the 8.0- and the 5.5-kb bands in the lung, and the 8.0-kb band in the intestine were detected (Figure 3D). We then examined the presence of the *Skt* and β-*geo* fusion mRNA (Figure 3E). In $Skt^{Gt/+}$ ES cells, an expected 10.5-kb band representing the fusion transcript containing β-*geo* was detected with both the *Skt* and *lacZ* probes, although the intensity was weaker than that of the 8-kb band of the endogenous transcript. In the $Skt^{Gt/+}$ and $Skt^{Gt/Gt}$ adult brains, two bands of 10.5 and 9.5 kb were detected with the *Skt* probe (Figure 3E, left), and these bands were also hybridized with the *lacZ* probe (Figure 3E, right), confirming that both transcripts corresponded to the fusion mRNA containing β-*geo*. This result indicates the existence of alternative splicing in the upstream region of the insertion site. Northern blot analysis using mRNA from wild-type adult heart revealed the presence of two different transcripts, the 7- and 5.5-kb bands when the *Skt* probe was used. However, in the Skt^{Gt} adult heart, one 9.5-kb band was detected with the *lacZ* probe (data not shown). This result indicates that alternative splicing in the heart may occur in the downstream region of the insertion site, leading to the production of the 7- and 5.5-kb bands. The largest size of mRNA is 8 kb, which is larger than that of the predicted cDNA sequence comprising 5930 nucleotides (accession no. AB125594). As described below, the anti-Skt antibodies recognized only an ~150-kDa protein corresponding to the predicted molecular weight of 147 kDa in extracts from the nucleus pulposus of the caudal IVDs (see lane 4 in Figure 6A). Thus, the 8-kb mRNA may contain untranslated regions at both the 5′- and 3′-ends and splicing may occur in each untranslated region. Further study will be required to determine the untranslated regions.

Formation of vertebral column and β-*geo* expression in Skt^{Gt} mice: We examined formation of the vertebral column in Skt^{Gt} mice during the embryonic, fetal, and postnatal periods (E8.0, E8.5, E9.0, E9.5, E10.5, E11.5, E12.5, E13.5, E14.5, 15.5, E16.5, E17.5, E18.5, E19.5, newborn, and 2 weeks of age) by histological analysis with and without X-gal staining. Before E8.0, the β-*geo* gene was expressed in the chorion, but not in the embryo (Figure 4A). At E8.5 (Figure 4B) and E9.0 (Figure 4C), intense staining was detected in the notochord. At E11.5, the notochord and the mesonephros expressed β-*geo* strongly (Figure 4, D–F). In addition, sections of E11.5 embryos showed β-*geo* expression in the epithalamus sulcus, roof of the neopallial cortex, lens vesicle, inner layer of retina, heart (atrium and ventricle), surface of hepatic primordium, infundiblum, surface ectoderm, hind gut, and mesenchyme of the limb bud (data not shown). No abnormality was found in both vertebral and intervertebral regions up to E16.5. In the $Skt^{Gt/Gt}$ embryo at E17.5, compression was observed in some IVDs (Figure 4, I and J) of the $Skt^{Gt/Gt}$ embryo, but not in the wild-type embryo (Figure 4, G and H). In the $Skt^{Gt/Gt}$ neonate, the X-gal-positive cells in the nucleus pulposus were shifted to the periphery and the alignment of the vertebral bodies was undulated (Figure 4, M and N). At this stage, sizes of IVDs are the same as those of wild-type mice. In 2-week-old $Skt^{Gt/Gt}$ mice, the X-gal-positive notochord cells were dislocated to the left or right side and the nuclei pulposi were smaller and eccentric, resulting in the disappearance of normal IVDs (Figure 4, Q and R). In the $Skt^{Gt/+}$ embryo and mice, the X-gal-positive cells were positioned in the center of the vertebrae at any stage (Figure 4, G, K, and O). Interestingly, the expression of the reporter gene was much lower in the upper IVDs than in the fifth to seventh caudal IVD, coinciding with a relationship between the phenotype of the $Skt^{Gt/Gt}$ and strong expression in the caudal region of the tail.

Histological analyses of IVDs of $Skt^{Gt/Gt}$ and *Sd* mutant adult mice: In $Skt^{Gt/Gt}$ adults, the β-*geo* gene was also expressed in many tissues such as the corpus callosum in the brain, uriniferous tubules in kidney, cardiac muscle, Sertoli's cells in testes, and basal cells and outer root sheaths of hair follicles in skin (data not shown).

In normal adult mice, the nucleus pulposus was located in the center of IVDs at all levels of the vertebral column (Figure 5, A, D, G, and J). However, the nucleus pulposus in the IVDs of the tail region of $Skt^{Gt/Gt}$ mice contained an aggregation of notochord-like cells with fewer vacuoles than normal and were dislocated to the periphery (Figure 5, H and K). The nucleus pulposus in the upper regions appeared normal (Figure 1, B and E). Although histochemical analyses of embryos and newborns in the *Sd* mutant were reported by Paavola *et al.* (1980) and Theiler (1988), the histochemical analyses of the IVDs in *Sd* mutant adult mice have not previously been performed in detail. Thus, we analyzed the IVDs of the whole spine in *Sd* +/+ + mutant mice. Surprisingly, the IVDs were totally occupied by peripheral fibers similar to those seen in the annulus fibrosus and no nucleus pulposus was found within the IVDs (Figure 5, C and F). The degeneration of the nucleus pulposus in the center of caudal IVDs was occasionally observed (Figure 5, I and L). Although tail kinks of $Skt^{Gt/Gt}$ mice were restricted to the 20–25th caudal vertebrae (Figure 1B), an irregular boundary with direct contact between the nucleus pulposus and annulus fibrosus (Figure 5, O and P) was observed in the 5–25th caudal IVDs of $Skt^{Gt/Gt}$ mice, compared to the sharp boundary and fixed space observed between the nucleus pulposus and the fibrous layers of the annulus fibrosus in normal mice (Figure 5, M and N). In addition to the abnormalities of the nucleus pulposus in IVDs, the annulus fibrosus development was also impaired in $Skt^{Gt/Gt}$ mice as demonstrated by the thin fibrous layers of annulus fibrosus and the failure of fibrous adhesion in the vertebral bodies (Figure 5, Q and R). We also examined whether similar abnormalities were

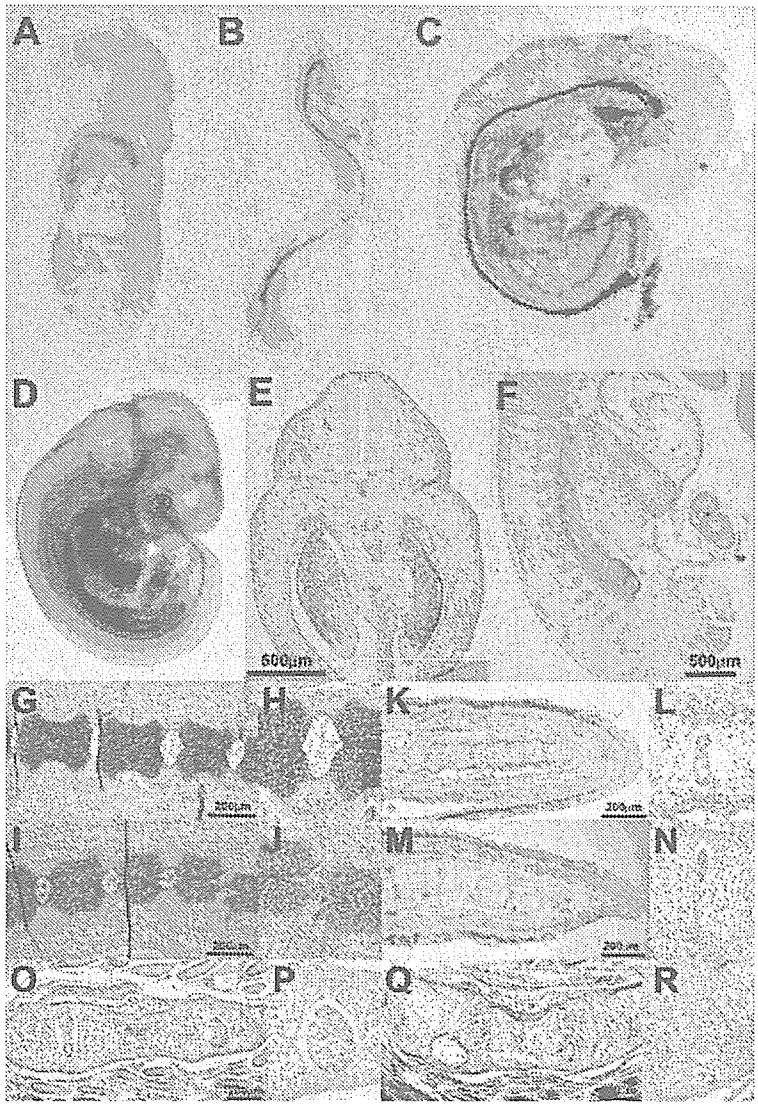

FIGURE 4.—β-*gal* expression and histological analyses in Skt^{Gt} mice. At E7.5 (A), the chorion was stained with X-gal, but the midline region of the embryo was not stained. At E8.5 (B) and E9.0 (C) intense staining was detected in the notochord. At E11.5 (D–F), the notochord and the mesonephros expressed β-*geo* strongly in whole-mount X-gal staining (D), the frontal section (E), and the sagittal section (F). Sagittal sections of the tail bud of $Skt^{Gt/+}$ (G and H) and $Skt^{Gt/Gt}$ (I and J) embryos at E17.5. At E17.5, some IVDs were compressed in the tail bud of $Skt^{Gt/Gt}$ (J). Sagittal sections of the tail tips of newborn $Skt^{Gt/+}$ (K and L) and $Skt^{Gt/Gt}$ (M and N) mice. In the $Skt^{Gt/Gt}$ neonate, the vertebral body alignment was undulated (M and N). Sagittal sections of the tail tips of 2-week-old $Skt^{Gt/+}$ (O and P) and $Skt^{Gt/Gt}$ (Q and R) mice. In the 2-week-old $Skt^{Gt/Gt}$ mice, the X-gal-positive nuclei pulposi were dislocated to the periphery (Q and R). (H, J, L, N, P, and R) Higher magnification of the area indicated by the boxes in G, I, K, M, O, and Q, respectively. Sections (G–J) were stained with alcian blue and sections of X-gal staining (E, F, and K–R) were counterstained with Nuclear Fast red. Bars, 200 μm.

observed in the regions that did not have kinks in $Skt^{Gt/Gt}$ mice (Table 1). Surprisingly, histological analysis of externally normal tails of $Skt^{Gt/Gt}$ mice revealed the presence of similar IVD abnormalities such as dislocation of the nucleus pulposus and thin fibrous layers of the annulus fibrosus (Figure 5S) as found in kinked tails (Figure 5, Q and R). This IVD phenotype was observed over 10 generations in the progeny backcrossed to C57BL/6. Thus, the primary phenotype of $Skt^{Gt/Gt}$ mice is the deformity of IVDs in the tail region. These histological pictures were clearly distinct from those of *Sd* mice.

Analysis of Skt protein using anti-Skt antibody: The anti-Skt antibodies recognized an ~150-kDa protein corresponding to the predicted molecular weight of 147 kDa in the lysates of BMT10 cells transiently expressing the *Skt* cDNA by the CAG promoter as well as in extracts from the nucleus pulposus of the caudal IVDs. No band was detected in extracts from untreated BMT10 cells and BMT10 cells transfected with mock expression vector (Figure 6A). This is consistent with the notion that ATG at positions 559–561 and TAA at positions 4615–4617 in the *Skt* cDNA are the start codon and termination codon, respectively. As expected, the amount of Skt protein was decreased in $Skt^{Gt/+}$ mice and was below the detectable level in $Skt^{Gt/Gt}$ mice (Figure 6A). After immunohistochemical staining, the nucleus pulposus cells from upper caudal vertebral discs were positively stained in wild-type mice (Figure 6B, a and c), but not in $Skt^{Gt/Gt}$ mice (Figure 6B, b and d). At higher magnification, the staining was observed mainly in the cytoplasm of the nucleus pulposus cells, indicating cytoplasmic localization of the Skt protein. Since we could not produce antibodies against the N terminus, the expression of the truncated protein was not confirmed in $Skt^{Gt/Gt}$ mice.

Relationship of *Skt* with $Etl4^{lacZ}$ or *Sd* loci: Both the expression pattern of the *Skt* gene and the phenotype of Skt^{Gt} mutant mice were quite similar to those of $Etl4^{lacZ}$ mutant mice (ZACHGO *et al.* 1998). Furthermore, by examining

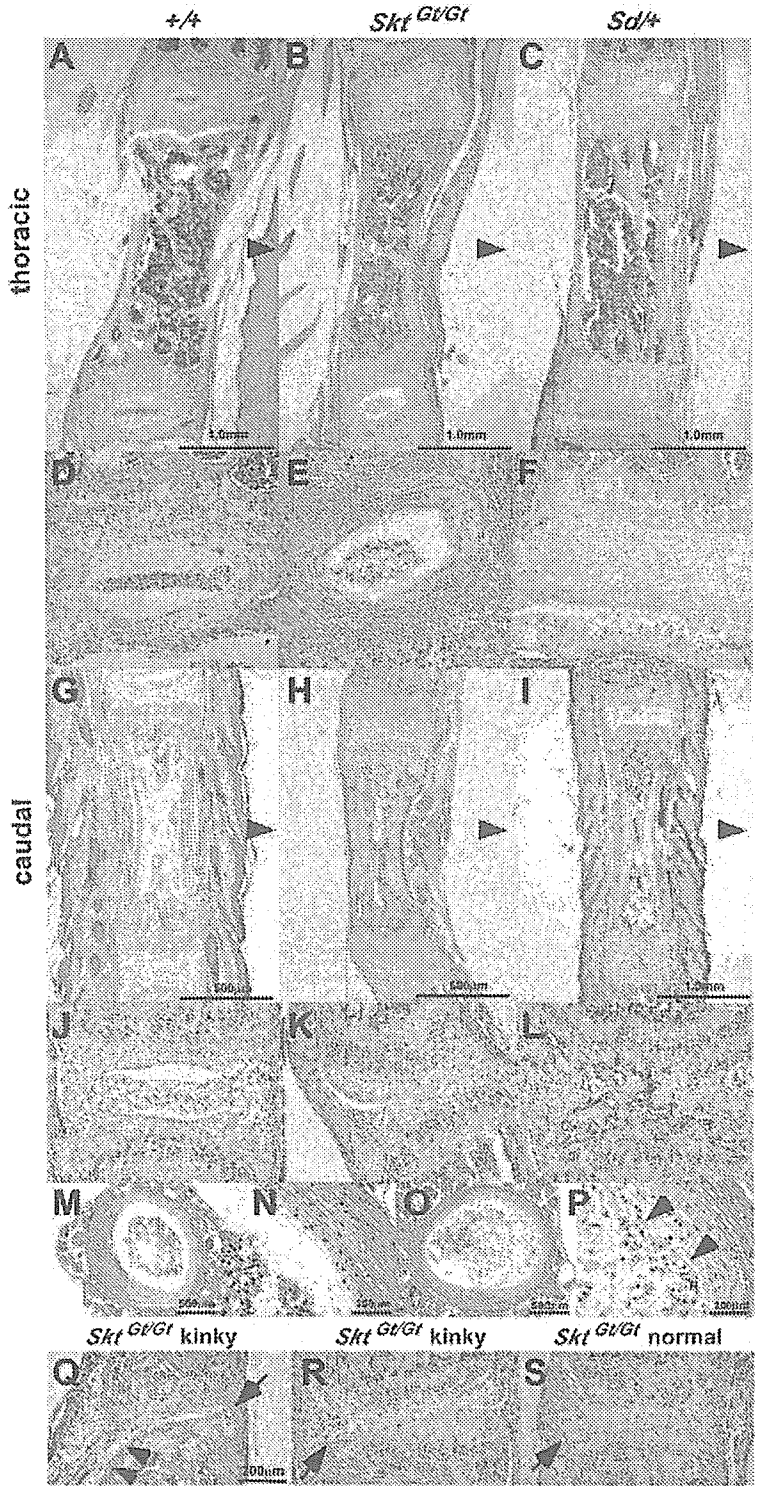

FIGURE 5.—Histological analyses of IVDs of $Skt^{Gt/Gt}$ and *Sd* mutant adult mice. Sagittal sections of the thoracic and caudal IVD from 8-week-old adult wild-type (A, D, G, and J), $Skt^{Gt/Gt}$ (B, E, H, and K), and heterozygous *Sd* mice (C, F, I, and L). (D, E, F, J, K, and L) Higher magnification of the area indicated by the boxes in A, B, C, G, H, and I, respectively. Arrowheads indicate the dorsal side. Axial sections of the upper caudal IVD in wild-type (M and N) and $Skt^{Gt/Gt}$ (O and P) 8-week-old mice. (N and P) Higher magnification of the area indicated by the boxes in M and O, respectively. The arrowheads in P indicate an irregular boundary with close contact between the nucleus pulposus and annulus fibrosus. (Q–S) The 20–25th caudal IVDs of $Skt^{Gt/Gt}$ 8-week-old mice. Impaired development of the annulus fibrosus in $Skt^{Gt/Gt}$ mice was demonstrated by the thin fibrous layers of annulus fibrosus (Q and R) and the failure of fibrous adhesion to the vertebral bodies (arrowhead in Q). Similar IVD abnormalities such as dislocation of the nucleus pulposus (arrow in Q–S) and impaired growth of the annulus fibrosus were observed in the nonkinked regions (S) and in the kinked regions (Q and S). Haematoxylin and eosin (HE) staining was used. Bars, 200 μm.

the reported primer sequences of the $Etl4^{lacZ}$ locus (MAATMAN *et al.* 1997), we found that the $Etl4^{lacZ}$ locus is located in the third intron of the *Skt* gene (Figure 2B) and that the distance between the integration sites of $Etl4^{lacZ}$ and Skt^{Gt} was 237 kb.

To examine the genetic distance and interaction between the Skt^{Gt} and *Sd* locus, we crossed Skt^{Gt} mice with *Sd* mice to produce the compound heterozygote (*Sd* +/+ Skt^{Gt}; *trans*-configuration). Then, these compound heterozygotes were used to analyze the recombination rate

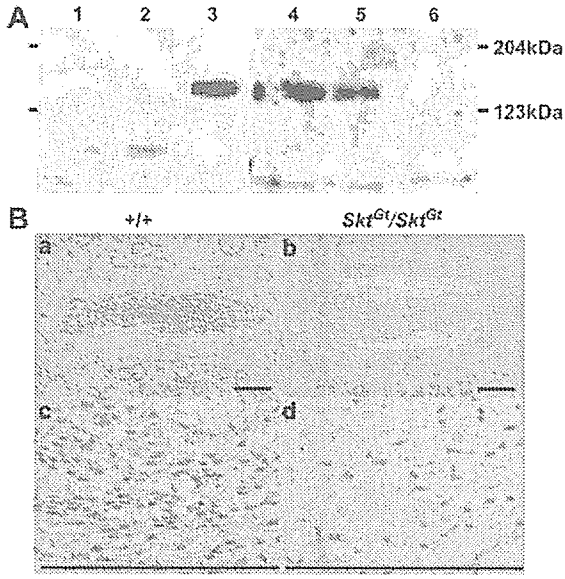

FIGURE 6.—Detection of the Skt protein. (A) Western blot analysis to detect Skt protein using extracts from untreated BMT10 cells (lane 1), BMT10 cells transfected with vector (lane 2), BMT10 cells transfected with the *Skt* expression vector (lane 3), and extracts of the nucleus pulposus of caudal IVDs from 8-week-old wild-type mice (lane 4), $Skt^{Gt/+}$ mice (lane 5), and $Skt^{Gt/Gt}$ mice (lane 6). An ~150-kDa protein corresponding to the predicted molecular weight of 147 kDa was detected in lanes 3, 4, and 5, but not in lane 6. The amount of Skt protein was reduced in the $Skt^{Gt/+}$ mutant (lane 5) and was below the detectable level in $Skt^{Gt/Gt}$ (lane 6). (B) Immunohistochemistry of frontal sections of the nucleus pulposus in upper caudal IVDs from adult 8-week-old mice using purified anti-Skt antibodies. Skt protein was detected in the cytoplasm of nucleus pulposus cells in wild-type (a and c), but not $Skt^{Gt/Gt}$, mice (b and d). (c and d) Higher magnification of the area indicated by the boxes in a and b, respectively. Bars, 200 μm.

between the two loci. As shown in Table 2, one compound heterozygote carrying the *Sd* mutation and the Skt^{Gt} insertion on the same chromosome (*Sd* Skt^{Gt}/+ +; *cis*-configuration) and two wild-type mice were obtained among 249 mice obtained by mating the *trans* compound heterozygote with the wild-type C57BL/6 mice, demonstrating that the *Sd* and Skt^{Gt} mutations were genetically separated. The genetic distance was calculated to be ~0.95 cM by combining the data from mating the [*Sd* Skt^{Gt}/+ +] (*cis*) compound heterozygote with the wild-type mice (Table 2).

To evaluate the effect of the Skt^{Gt} mutation on the tail phenotype in heterozygous *Sd* mice in either the *trans*- or the *cis*-configuration, the number of vertebrae was determined by X-ray analysis. Heterozygous *Sd* [*Sd* +/+ +] mice (n = 22) had a variable number of vertebrates and the vertebral columns were truncated at the sixth caudal vertebral body on average. Both *trans* [*Sd* +/+ Skt^{Gt}] (n = 23) and *cis* [*Sd* Skt^{Gt}/+ +] (n = 10) compound heterozygous mice had shorter tails, in which the vertebral columns were truncated at the second and third caudal vertebral body on average (Figure 7A). We examined whether the phenotype of [*Sd* Skt^{Gt}/+ Skt^{Gt}] neonatal mice is more severe than those of *trans* [*Sd* +/+ Skt^{Gt}] and *cis* [*Sd* Skt^{Gt}/+ +] compound heterozygous mice. Approximately 80% of [*Sd* Skt^{Gt}/+ Skt^{Gt}] neonatal mice died within 48 hr of birth and all mutant mice died within 2 weeks. In addition, as shown by making alcian blue/alizarin red whole-mount preparations of [*Sd* Skt^{Gt}/+ Skt^{Gt}] neonatal mice, [*Sd* Skt^{Gt}/+ Skt^{Gt}] neonatal mice had shorter tails than those of *trans* [*Sd* +/+ Skt^{Gt}] and *cis* [*Sd* Skt^{Gt}/+ +] compound heterozygous mice, in which the vertebral columns were truncated at the fourth sacral vertebral body on average, suggesting a cumulative effect of the Skt^{Gt} mutation on the *Sd* mutant.

To examine the pathologic effect of the *Skt* mutation on the *Sd* phenotype, we carried out histological analyses on the IVDs of *Sd* +/+ Skt^{Gt} and *Sd* Skt^{Gt}/+ + mutant mice. Both compound heterozygous mice showed IVD histology similar to that seen in *Sd* +/+ + mutant mice. The nucleus pulposus was totally absent and replaced by peripheral fibers similar to those seen in the annulus fibrosus in all IVDs (Figure 7B, a–h). These results suggest that the *Skt* mutation did not affect the histological picture of IVD in the *Sd* mutation. In addition, the expression pattern of the β-*geo* gene in the tail notochord was the same in both *trans* [*Sd* +/+ Skt^{Gt}] and *cis* [*Sd* Skt^{Gt}/+ +] compound heterozygous embryos at E9.5 and E13.5 (Figure 7C). The notochord of both *trans* and *cis* compound heterozygous embryos was thin and clearly stained at E9.5 (Figure 7C, a and d), and the X-gal-positive notochord was similarly fragmented in both *trans* and *cis* compound heterozygous embryos at E13.5 (Figure 7C, b, c, e, and f). This suggested that the *Sd* mutation did not affect *Skt* expression. In addition, this *trans–cis* test demonstrated that the double heterozygotes exhibited indistinguishable phenotypes in

TABLE 2

Distribution of the haplotypes among the 315 offspring of the backcross *Sd* +/+ Skt^{Gt} or *Sd* Skt^{Gt} /+ + × C57BL/6

Sd +/+ Skt^{Gt} × C57 BL/6				*Sd* Skt^{Gt}/+ + × C57 BL/6			
+ +/+ Skt^{Gt}	*Sd* +/+ +	*Sd* Skt^{Gt}/+ +	+ +/+ +	+ Skt^{Gt}/+ +	*Sd* +/+ +	*Sd* Skt^{Gt}/+ +	+ +/+ +
144	102	1	2	0	0	24	42

Sd, Skt^{Gt} compound heterozygotes were generated from crosses with an inbred laboratory strain (C57BL/6)

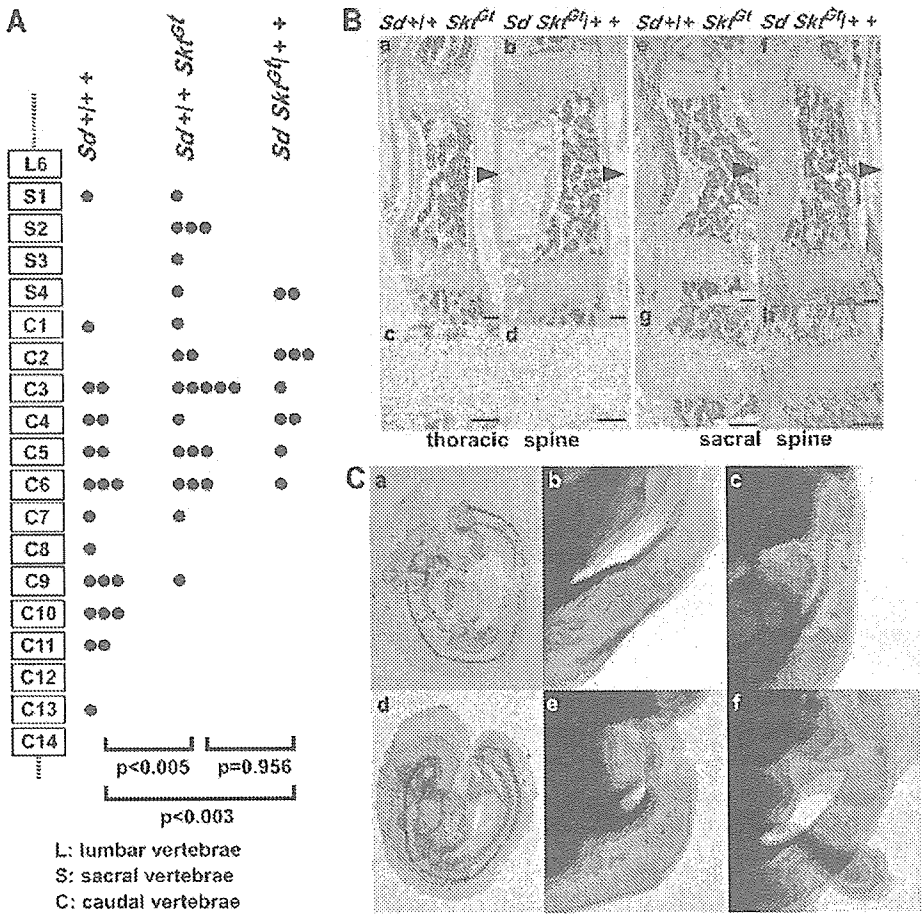

FIGURE 7.—(A) Schematic of axial levels and severity of vertebral malformations in compound mutant 8-week-old mice. A single solid circle indicates the level of the terminal vertebral body for a single mouse. In both *trans* and *cis* compound mutant mice, the degree of vertebral malformation is more severe than that in heterozygous *Sd* mice (*trans*, $P < 0.005$; *cis*, $P < 0.003$, Mann–Whitney *U*-test). There was no significant difference between *trans* [*Sd* +/+ Skt^{Gt}] ($n = 23$) and *cis* [*Sd* Skt^{Gt}/+ +] ($n = 10$) mice ($P = 0.956$, Mann–Whitney *U*-test). (B) Histological analyses of vertebral columns in the *Sd* +/+ Skt^{Gt} and *Sd* Skt^{Gt}/+ + mutant mice. HE staining of midsagittal sections in thoracic spines of *Sd* +/+ Skt^{Gt} (a and c) and *Sd* Skt^{Gt} /+ + (b and d) mice and in sacral spines of *Sd* +/+ Skt^{Gt} (e and g) and *Sd* Skt^{Gt}/+ + (f and h) mice. Arrowheads indicate dorsal sides. (c, d, g, and h) Higher magnification of the areas indicated by the boxes in a, b, e, and f, respectively. (C) Whole-mount X-gal staining in the *Sd* +/+ Skt^{Gt} and *Sd* Skt^{Gt}/+ + mutant embryos. The β-*gal* expression in the tail notochord of *trans*-heterozygous embryos [*Sd* +/+ Skt^{Gt}] at E9.5 (a) and E13.5 (b and c) and of *cis*-heterozygous embryos [*Sd* Skt^{Gt}/+ +] at E9.5 (d) and E13.5 (e and f).

regard to notochord degradation whether *Sd* and Skt^{Gt} were in a *trans*- or in a *cis*-configuration.

DISCUSSION

We established a new recessive trap line, B6;CB-$Skt^{Gt(yn8021)IMEG}$, which had a deformity in caudal IVDs. The insertion site of the trap vector is in the 14th intron of the novel gene *Skt*, located on chromosome 2, near the locus for *Danforth's short tail*. In addition, we found that the enhancer trap locus $Etl4^{lacZ}$, which was previously reported to be an allele of *Sd*, was located in the third intron of the *Skt* gene.

Structure, expression, and function of the *Skt* gene: The sequence of the trapped gene, *Skt*, was obtained using the gene-trap ES clone. The *Skt* gene contains 19 exons encoding a novel protein of 1352 amino acids with a proline-rich region in the N terminus (amino acid positions 298–364) and a coiled-coil domain in the middle (amino acid positions 626–656). Although the role of the proline-rich region in many proteins is not clear yet, a proline-rich region located in the amino-terminal region has been shown to be important for proper folding in cytochrome P450s (mitochondrial, microbial, and microsomal P450s) (KUSANO *et al.* 2001a,b). Thus, the proline-rich region in the Skt protein may have a similar function in protein folding. The coiled-coil motif was first described by CRICK (1952) and by PAULING and COREY (1953) as the main structural element of a large class of fibrous proteins that included keratin, myosin, and fibrinogen, mediating dimerization, heterodimer formation, or trimerization (for a review see LUPAS 1996). These proteins provide a scaffold for regulatory complexes such as tropomyosin and a protective surface for pathogens. As the Skt protein is localized in the cytoplasm, it is conceivable that the Skt protein may provide structural elements or act as a scaffold for regulatory complexes.

Insertion of the gene-trap vector into the 14th intron of the *Skt* gene, downstream of the coiled-coil domain and the proline-rich region, resulted in production of two fusion transcripts with the β-*geo* sequence: one, *Skt-a*,

containing only exons 1–14 and the other, *Skt-b*, lacking 33 bp of the 13th exon from *Skt-a* (see Figure 2B). Northern blot analysis showed that the amount of fusion transcripts from the trapped allele was lower than that of the wild-type allele. Therefore, it is also possible that the insertion of the gene-trap vector resulted in decreased mRNA stability. As tail phenotypes are recessive, insertion of the trap vector may cause a hypomorphic or null mutation, but not a dominant-negative mutation. Although we detected four types of mRNA transcribed from the wild-type *Skt* allele, further analysis will be required to elucidate the function of these mRNA.

The expression patterns of the *Skt* gene can be monitored by X-gal staining, because the expression of the reporter gene, β-*geo*, is under control of the regulatory region of the *Skt* gene. At E11.5, β-*geo* was expressed mainly in the notochord and mesonephros at high levels, and in other tissues as described in the RESULTS. In the $Etl4^{lacZ}$ line, the *lacZ* reporter gene was also expressed in two main tissues, the notochord and the mesonephros (ZACHGO *et al.* 1998). In both lines, *lacZ* expression was first detected at E8.5 in the presumptive notochord cells. In the $Etl4^{lacZ}$ line, *lacZ* expression was detected in the future IVDs at E13.5 and persisted up to E14.5. However, no *lacZ* expression was detected in the IVDs of newborn and adult mice. On the other hand, *lacZ* expression in the IVDs persisted to adult stage in the Skt^{Gt} line. These results suggest that the enhancer located near the $Etl4^{lacZ}$ locus is not sufficient to express the *lacZ* gene in the IVDs of adult mice.

Histochemical analyses of the vertebral column revealed the differences between *Sd* mice and Skt^{Gt} mice. As histological data on $Etl4^{lacZ}$ mice were not described by ZACHGO *et al.* (1998), it is not clear whether the IVD histology is similar to that seen in *Sd* or Skt^{Gt} mice. As reported previously, the development of both the vertebral column and the urogenital system is affected in *Sd* mutation, suggesting that the *Sd* gene is required for formation of derivatives from both the paraxial and the intermediate mesoderm. In addition, both vertebral bodies and IVDs are affected in *Sd* mice. The notochord shows discontinuities as early as E9.5, resulting in the total absence of the nucleus pulposus at all levels and is replaced by peripheral fibers similar to those of the annulus fibrosus in *Sd* adult mice. All vertebral bodies are reduced in a dorso-ventral direction and the number of tail vertebrae is reduced, leading to shortening or absence of the tail. However, in Skt^{Gt} mice, the compression and dislocation of the nucleus pulposus were first observed at E17.5 and were restricted to the tail region. Interestingly, the size of the nucleus pulposus was similar to that in wild-type mice until birth. After birth, the nucleus pulposus did not expand and was dislocated to the periphery, resulting in a kinky-tail phenotype in adults. These observations suggest that *Sd* acts at an early stage of mesoderm development involving both sclerotome and notochord development and that *Skt* acts during the fetal period and at the later stage involving growth and hypertrophy of the nucleus pulposus. Although massive apoptosis in notochord cells was observed in embryos with targeted disruption of *Jun* (BEHRENS *et al.* 2003) or $Sox5^{-/-}/Sox6^{-/-}$ (SMITS and LEFEBVRE 2003), no apoptotic notochord cells were observed in the $Skt^{Gt/Gt}$ embryos at E16.5 and in neonatal mice. Thus, apoptosis is not the cause of compression or dislocation of the nucleus pulposus in Skt^{Gt} mice. As the Skt protein contains the coiled-coil motif that is involved in the formation of mechanically rigid structures, it is possible that the nucleus pulposus lacking Skt protein may not be capable of sustaining mechanical loads, leading to compression or dislocation of the nucleus pulposus.

Although the IVD is formed from two components of developmentally different origins, the nucleus pulposus and the annulus fibrosus, interaction of the nucleus pulposus and annulus fibrosus is not clear yet. In *Sd* mice, disappearance of the notochord cells occurs at early stages of development. THEILER (1988) reported that the fibers of the annulus fibrosus are reduced in *Sd* heterozygous embryos and newborns. However, our results suggest that the annuli fibrosi are not reduced in *Sd* heterozygous adult mice. Thus, the annulus fibrosus may be able to completely compensate for the loss of the nucleus pulposus during growth after birth. In Skt^{Gt} mice, the thin annulus fibrosus was observed together with abnormalities in the nucleus pulposus. At present, it is not known whether the thin annulus fibrosus is caused by the direct effect of *Skt* deficiency or indirectly caused by defects in the nucleus pulposus.

The relationship among the Skt^{Gt}, $Etl4^{lacZ}$, and *Sd* mutations: Our breeding studies revealed that the genetic distance between the *Skt* and *Sd* loci was 0.95 cM. We believe that the *Skt* gene is distinct from the *Sd* gene for the following reasons. First, anti-Skt antibody detected the predicted size of protein deduced from the *Skt* gene. If the *Skt* was part of the *Sd* gene, we should have detected a larger protein by Western blot analysis. But, we could not detect any such protein. Second, our *trans–cis* test demonstrated that both double heterozygotes exhibited indistinguishable phenotypes, regardless of whether *Sd* and Skt^{Gt} were in a *trans*- or a *cis*-configuration. On the basis of the results by ZACHGO *et al.* (1998), *Sd* is a gain-of-function mutation. As the *Skt* is a recessive mutation, producing a hypomorphic or null allele, the *Sd* phenotype is expected to be attenuated in the *cis*-configuration. Therefore, the phenotype in double heterozygotes in the *trans*-configuration might be more severe than that in the *cis*-configuration if the *Skt* gene is part of the *Sd* gene.

We have shown that the $Etl4^{lacZ}$ locus is located in the third intron of the *Skt* gene. Interestingly, a sequence that has 93% homology to consensus sequence 3 (CS3) in node/notochord enhancers of *Hnf3*β (NISHIZAKI *et al.* 2001) was found in the fourth intron of the *Skt* gene, located 106 kb downstream of the insertion site of